ASSEMBLY OF MAGNETIC NANOPARTICLES INTO HIGHER STRUCTURES ON PATTERNED MAGNETIC BEADS UNDER INFLUENCE OF MAGNETIC FIELD

by
Tuğçe Özdemir

Submitted to the Institute of Graduate Studies in
Science and Engineering in partial fulfillment of
the requirements for the degree of
Master of Science in Chemical Engineering

Yeditepe University
2010

ASSEMBLY OF MAGNETIC NANOPARTICLES INTO HIGHER STRUCTURES ON PATTERNED MAGNETIC BEADS UNDER INFLUENCE OF MAGNETIC FIELD

APPROVED BY:

Assist. Prof. Seyda Bucak (Supervisor) .....

Assist. Prof. Erde Can .....

Assist. Prof. Amitav Sanyal .....

DATE OF APPROVAL: …./…./….

ACKNOWLEDGEMENTS

It would not have been possible to write this thesis without the help and support of the kind people around me, to only some of whom it is possible to give particular mention here.

First of all, I would like to express my deepest gratitude to my advisor, Assist. Prof. Seyda Bucak, for her excellent guidance, care and patience. She always supported me whenever I needed encouragement. I also thank to all the members of the Tübitak Project, Prof. Naz Zeynep Atay, Assoc. Prof. Mustafa Çulha, Assist. Prof. Amitav Sanyal. I also would like to thank to Deniz Sandal for her friendship and preparing templates for the micropatterning.

Special thanks to my laboratory friends, Ela Bilginoğlu, Binnaz Coşkunkan, Ayşe İrem Kanneci, Gökçe Üdenir and Merve Yüksel for their friendship. They were always there when I needed help. I have to thank to Cem Levent Altan for his friendship and teaching me when I started this project. Also, I would like to thank to Metin Hacıoğlu for his continuous support and encouragement.

Finally I am grateful to my family for their love, patience and understanding not only during the project but also throughout my life.

This project was financially supported by TUBITAK Grant number 107M580.

ABSTRACT

ASSEMBLY OF MAGNETIC NANOPARTICLES INTO HIGHER STRUCTURES ON PATTERNED MAGNETIC BEADS UNDER INFLUENCE OF MAGNETIC FIELD

The self-assembly of nanoparticles (NPs) into higher organizations in a controlled manner has critical importance for the utility of the unique properties of NPs. Magnetic nanoparticles, Fe_3O_4, (MNPs) also show unique properties and can be manipulated under the influence of a magnetic field. Therefore, in order to build higher structures MNPs are used and manipulated in the presence of an external magnetic field. In this study, after the synthesis of MNPs with an average size of 6 nm, the influence of template and solvent which MNPs were suspended in, are investigated on the controlled assembly of MNPs on various surfaces by drop casting. Compact Discs (CD) are used as the template to create patterned surfaces with magnetic beads. When an external magnetic field is applied, magnetic beads which are magnetic nanoparticles embedded in a polymer matrix, exaggerate the magnetic field gradient and therefore increase the magnetic force acting on the solvent allowing the ability to align the MNPs during solvent evaporation. Different templates and different solvents are successfully used and tested in both absence and presence of magnetic field. It is found that upon evaporation of the solvent where the MNPs are suspended, formation of unique micrometer sized structures is achieved only when there is a patterned surface constructed from sub-micrometer size magnetic beads in between the applied magnetic field and MNPs. The preliminary results indicate that the combined effect of magnetic field and evaporation rate might help the control of NP behavior on surfaces and interfaces to construct higher structures. This work may offer a new and simple approach for preparation of patterned and renewable surfaces, constructed from MNPs, which find use in many fields of science and technology.

ÖZET

MANYETİK NANOPARÇACIKLARIN MANYETİK ALAN ETKİSİYLE MANYETİK BONCUKLARLA OLUŞTURULMUŞ ÖRÜNTÜLER ÜZERİNDE YÜKSEK YAPILAR OLUŞTURMASI

Nanoparçacıkların (NP) kontrollü olarak daha büyük yapılara derlenmelerinin NP'lerin özgün özelliklerinin yararları açısından büyük önemi vardır. Ayrıca manyetik nanoparçacıklar da, Fe_3O_4, (MNPs) özgün özellikler göstermekle birlikte manyetik alan etkisi altında hareket ettirilebilirler. Dolayısıyla daha büyük yapılar oluşturmak için MNP'ler kullanılmıştır ve harici manyetik alan varlığında idare edilmiştir. Bu çalışmada, ortalama boyutları 6 nm olan MNP'lerin sentezinden sonra, alt örüntünün ve MNP'lerin süspanse edildikleri çözücünün etkisi araştırılmıştır. Kompakt diskler (CD), manyetik boncuklarla birlikte örüntülü yüzeyler oluşturmak için kullanılmışlardır. Harici manyetik alan uygulandığında, manyetik nanoparçacıkların polimer matriksine sokularak oluşturulmuş manyetik boncuklar, manyetik alan şiddetini artırırlar ve böylece çözücü üzerine etki eden manyetik kuvveti artırırlar. Çözücü üzerindeki manyetik kuvvet artışı MNP'lerin çözücü buharlaşması sırasında hizalanma yeteneklerine izin verir. Farklı örüntüler ve farklı çözücüler başarı ile çalışılmış olup hem manyetik alan varlığında hem de yokluğunda test edilmiştir. MNP'lerin süspanse edildikleri çözücünün buharlaşmasıyla, sadece manyetik boncuklarla oluşturulmuş örüntülü yüzeylerde özgün mikrometre boyutlarında yapıların elde edildiği bulunmuştur. İlk sonuçlar buharlaşma hızı ile manyetik alanın birleşmiş etkisinin NP'lerin yüzeyler ve arayüzler üzerinde daha büyük yapılar meydana getirmesine yardımcı olabileceğini göstermektedir. Bu çalışma bilim ve fenin çoğu alanında kullanılan MNP'lerden örüntülü ve yenilenebilir yüzeylerin hazırlanması için yeni ve basit bir yaklaşım sunabilir.

TABLE OF CONTENTS

ACKNOWLEDGEMENTS iii
ABSTRACT iv
ÖZET v
TABLE OF CONTENTS vi
LIST OF FIGURES viii
LIST OF TABLES xii
LIST OF SYMBOLS / ABBREVIATIONS xiii
1. INTRODUCTION 1
2. THEORETICAL BACKGROUND 4
2.1. NANOTECHNOLOGY 4
2.2. MAGNETIC NANOPARTICLES (MNP) 6
2.2.1. Superparamagnetism 8
2.2.2. Synthesis Methods 10
2.2.3. Applications of Magnetic Nanoparticles 12
2.3. GOLD COATED MNPs (CORE/SHELL) 13
2.4. SELF-ASSEMBLY 15
3. MATERIALS AND METHODS 18
3.1. CHEMICALS 18
3.2. CHEMICALS AND MATERIALS FOR TEMPLATE PREPARATION 20
3.3. CHARACTERIZATION METHODS 22
3.3.1. Dynamic Light Scattering (DLS) 22
3.3.2. X-Ray Diffraction (XRD) 24
3.3.3. Transmission Electron Microscope (TEM) 25
3.3.4. Scanning Electron Microscope (SEM) 27
4. SYNTHESIS AND CHARACTERIZATION OF MNPs 29
4.1. SYNTHESIS OF HYDROPHOBIC MNPs 29
4.2. SYNTHESIS OF GOLD COATED HYDROPHOBIC MNPs 31
4.3. SYNTHESIS OF HYDROPHILIC MNPs 31
4.4. IRON TEST FOR DETERMINING MAGNETITE CONCENTRATION 32

4.5. DISPERSING THE PARTICLES PREPARED BY OIL SYNTHESIS IN WATER 33
4.6. CHARACTERIZATION OF MNPs 34
4.6.1. Characterization of Hydrophobic MNPs 35
4.6.2. Characterization of Gold Coated Hydrophobic MNPs 37
4.6. CONCLUSION 39
5. MICROPATERNING OF SYNTHESIZED MNPs 40
5.1. TEMPLATE PREPATION 41
5.2. TEMPLATING STUDIES 42
5.3. CHARACTERIZATION OF MICROPATTERNED MNPs 43
5.3.1. MNP Solution on Untreated CD Surface 43
5.3.2. MNP Drop Casting on Patterned CD 46
5.3.3. MNP Drop Casting on Patterned CD with PDMS 49
5.3.4. Gold Coated MNP Drop Casting on Patterned CD with PDMS 55
5.4. CONCLUSION 57
6. CONCLUSION AND RECOMMENDATIONS 59
6.1. CONCLUSION 59
6.2. RECOMMENDATIONS 61
REFERENCES 62

LIST OF FIGURES

Figure 2.1. The schematic representation of bottom-up and top-down methods 4

Figure 2.2. a. Lycurgus Cup, Roman Era (4th Century A.D). It appears green in reflectected light and red in tansmitted ligth. It contains gold and silver particles of app. 70 nm, b. and in the ratio 1:14..... 5

Figure 2.3. Crystal structures of a. hematite, b. magnetite..... 8

Figure 2.4. The response of MNPs to the presence and absence of magnetic field 9

Figure 2.5. Superparamagnetic particles a. under the influence of an external magnetic field, b. in absence of an external magnetic field, monodisperse particle distribution..... 10

Figure 2.6. Ag/Au core/shell nanoparticles..... 14

Figure 2.7. Effect of shell on properties of NPs..... 14

Figure 3.1. MBs 21

Figure 3.2. Hydrodynamic diameter measured by DLS..... 23

Figure 3.3. X-ray diffraction..... 25

Figure 3.4. Individual parts of a typical TEM 26

Figure 3.5. The schematic illustration of SEM..... 27

Figure 3.6. The visible region for EMs and light microscopes 28

Figure 4.1. Experimental set-up for synthesis of hydrophobic MNPs 30

Figure 4.2. Experimental set-up for synthesis of hydrophilic MNPs 32

Figure 4.3. TEM image of hydrophobic MNPs 35

Figure 4.4. DLS image for hydrophobic synthesis of MNPs 35

Figure 4.5. Characteristic XRD peaks of MNPs 36

Figure 4.6. XRD graph of hydrophobic MNPs 37

Figure 4.7. TEM images of gold coated hydrophobic MNPs 38

Figure 4.8. XRD graph of gold coated hydrophobic MNPs 39

Figure 4.9. XRD peaks of Au-Fe 39

Figure 5.1. The convective-assembly set up 41

Figure 5.2. The schematic representation of the overall experiments: a. the CD template having microchannels, b. assembled beads into the microchannels, c. covered substrate with a thin film o f PDMS, d. dropping MNPs under the magnetic field 42

Figure 5.3. Side view of CD on top of a magnet 43

Figure 5.4. MNPs suspended in n-heptane on untreated CD (magnetic field on) 44

Figure 5.5. MNPs suspended in n-heptane on untreated CD (magnetic field off) 45

Figure 5.6. MNPs suspended in n-decane on untreated CD (magnetic field on) 45

Figure 5.7. MNPs suspended in n-decane on untreated CD (magnetic field off)..... 46

Figure 5.8. Side view of CD with MBs on top of a magnet..... 47

Figure 5.9. MBs in the microchannels 47

Figure 5.10. MBs on CD (magnetic field on) 48

Figure 5.11. MNPs suspended in n-heptane on MBs (magnetic field on)..... 48

Figure 5.12. MNPs suspended in n-heptane on MBs (magnetic field off)..... 49

Figure 5.13. Side view of CD with MBs fixed with PDMS on top of a magnet 49

Figure 5.14. a. MBs in the microchannels, b. MBs covered with PDMS 50

Figure 5.15. MNPs in n-heptane on CD (patterned MBs covered with PDMS) (magnetic field on) 51

Figure 5.16. MNPs in n-heptane on CD (patterned MBs covered with PDMS) (magnetic field on) 52

Figure 5.17. MNPs in n-heptane on CD (patterned MBs covered with PDMS) (magnetic field off)..... 52

Figure 5.18. MNPs in n-decane on CD (patterned MBs covered with PDMS) (magnetic field on) 53

Figure 5.19. MNPs in n-decane on CD (patterned MBs covered with PDMS) (magnetic field on) 54

Figure 5.20. MNPs in n-decane on CD (patterned MBs covered with PDMS) (magnetic field off)..... 54

Figure 5.21. MNPs in n-hexane on CD (patterned MBs covered with PDMS) (magnetic field on) 56

Figure 5.22. MNPs in n-hexane on CD (patterned MBs covered with PDMS) (magnetic field off) 56

Figure 5.23. MNPs in water on CD (patterned MBs covered with PDMS) (magnetic field on) 57

Figure 5.24. Gold coated MNPs in n-decane on CD (patterned MBs covered with PDMS) (magnetic field on) 58

Figure 5.25. Gold coated MNPs in n-decane on CD (patterned MBs covered with PDMS) (magnetic field off)..... 59

LIST OF TABLES

Table 2.1. Physical and magnetic properties of iron oxides 7

Table 3.1. Chemicals for synthesis of hydrophobic MNPs..... 18

Table 3.2. Chemicals for synthesis of hydrophilic MNPs 19

Table 3.3. Chemicals for synthesis of gold coated hydrophobic MNPs..... 19

Table 3.4. Chemicals used as solvents..... 19

Table 3.5. Chemicals used for iron test..... 20

Table 3.6. Chemicals for synthesis of hydrophilic MNPs from hydrophobic MNP's 20

Table 3.7. The properties of the MBs 21

Table 4.1. Conversion formulation for 480 mg of magnetite nanoparticles 34

LIST OF SYMBOLS / ABBREVIATIONS

AFM	Atomic force microscopy
AuNP	Gold nanoparticle
CD	Compact disc
EM	Electron microscopy
MB-a	Amine functionalized magnetic beads
MB-c	Carboxyl functionalized magnetic beads
MBs	Magnetic beads
MNPs	Magnetic nanoparticles
NPs	Nanoparticles
PDMS	Poly dimethyl siloxane
SEM	Scanning electron microscopy
T	Tesla
TEM	Transmission electron microscopy
XRD	X-ray diffraction

1. INTRODUCTION

Nanotechnology is an engineering discipline that applies methods from nanoscience to create usable, marketable, and economically viable products. It is the ability to work at the molecular level, atom by atom, to create large structures with fundamentally new molecular organizations. The assembly of nanoparticles (NPs) into organized structures and patterns is of paramount importance in many areas of modern science and technology with applications ranging from the production of integrated circuits, information storage devices and display units to the fabrication of micro-electromechanical systems (MEMS), miniaturized sensors, micro-optical components and diffractive optical elements [1]. A major effort in nanotechnology has been devoted to the patterning of active materials into size and shape controlled structures, because of the ambitious goal of controlling physical properties through the control of materials' length scales [2]. For most of these applications the fabrication of thin films and/or artificially organized patterns are certainly a crucial issue [3].

Magnetic nanoparticles (MNPs) have emerged as an important building block in nanobiotechnology since they can be obtained in sizes comparable to those of a protein, antibody, DNA or RNA, and can interact with or bind to such biomolecules. Their magnetic properties lead to magnetic carriers for biomedical applications such as DNA and RNA purification, cell separation, magnetic drug delivery, hyperthermia and magnetic resonance imaging (MRI) contrast enhancement [4-7]. Much effort has been focused on obtaining patterned arrays comprised of MNPs. Towards this end, earlier work has reported the use of microcontact printing [8] combined with layer-by-layer self-assembly [9], and applying electron beam treatment to the formed layers of NPs [10] as well as focused ion beams [11].

Recent developments indicate that the application of a magnetic field could be an elegant way to orient and self-assemble magnetic particles into nano- and micro-scale structures, in which dipole–dipole interactions between adjacent magnetic NPs force them to form reversible anisotropic structures [12-15].

Superparamagnetism is a form of magnetism, which is observed with small ferromagnetic or ferrimagnetic NPs. Superparamagnetism occurs in NPs that have single-domain, i.e. composed of a single magnetic domain. In this condition, it is considered that the magnetization of the NPs is a single-giant magnetic moment, the sum of all the individual magnetic moments carried by the atoms of the NP. When an external magnetic field is applied to the superparamagnetic NPs, they tend to align along the magnetic field, leading to a net magnetization. In the absence of an external magnetic field, however, the dipoles are randomly oriented and there is no net magnetization [17].

In this study, the aim is to to prepare well-defined magnetic surfaces and to investigate their use as chemical and biological sensors, as well as in the development of various diagnostic methods. For this purpose, a template consists of pre-existing channels of a commercial CD is used. The channels are roughly filled with micrometer size beads composed of MNPs embedded in a polymer matrix (Ademtech® beads with an average size of 500 nm). The CD channels filled with microbeads are then coated with a thin layer of polydimethylsiloxane (PDMS) to ensure the beads to stay inside the channels. The surface is exposed to a suspension containing superparamagnetic NPs. A combination of magnetic accentuation of microbeads by application of external magnetic field, coupled with superparamagnetism of MNPs and solvent evaporation leads to well-defined hierarchical structures of densely packed standing cylinders composed of MNPs.

General information about nanotechnology, MNPs and synthesis methods, core and shell structures, gold coated MNPs as well as the self assemble are given in the theoretical background part of the report. In Chapter 3 materials and chemicals as well as the characterization techniques are introduced which were used during the project. Furthermore, in Chapter 4 synthesis methods of magnetite and the characterization results are given with discussions. Finally, Chapter 5 includes both the methods and the results of micropatterning of synthesized MNPs. Chapter 6 gives a general summary of the conclusions of the thesis and recommendations for future work.

2. THEORETICAL BACKGROUND

2.1. NANOTECHNOLOGY

Nanotechnology is based on the prefix “nano” which is from the Greek word meaning “dwarf”. In more technical terms; the word “nano” means one billionth of meter or to put it comparatively, about 1/80 000 of the diameter of a human hair. The word nanotechnology is generally used when referring to materials with the size of 0.1 to 100 nanometers.

Nanotechnology is the manipulation or self-assembly of individual atoms, molecules, or molecular clusters into structures to create materials and devices with new or vastly different properties. Materials that are in the size range 10-100 nm can be prepared by using two techniques, the top-down and the bottom-up methods as it can be seen from the Figure 2.1. The top-down technique is applied to process macro-scale materials into smaller sizes, whereas the bottom-up method is applied to integrate molecules or atoms into nano-scale materials [18].

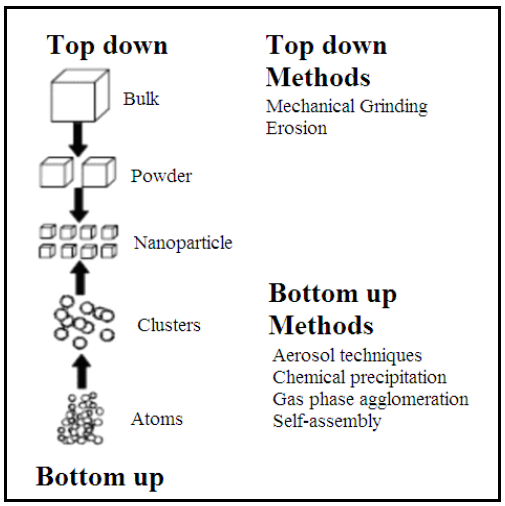

Figure 2.1. The schematic representation of bottom-up and top-down methods [18]

Potential nanotechnological applications in the next few decades could produce huge increases in computer speed and storage capacity, therapies for several different types of cancer, much more efficient lighting and battery storage, a major reduction in the cost of desalinating water, clothes that never stain and glass that never needs cleaning [19].

To build materials by bottom-up approach, the first requirement is to have clusters of the material consisting of a few ($3\text{-}10^7$) molecules. One such system of clusters of particles is the colloidal system. Colloids can be defined as: “a mixture with properties between those of a solution and fine suspension”. Colloidal systems have been known and exploited for centuries in diverse areas ranging from pigments and paints to medicines, as well as in photography, agriculture, etc. The Lycurgus Cup from the Roman times owes its unique property of appearing green in reflected light and red in transmitted light due to nanometric gold and silver particles in glass (Figure 2.2). Colloids can be composed of particles of a wide range of sizes from a few micrometers as in the colloidal system that forms milk, to a few nanometers as in the colloidal system in the Lycurgus Cup. For ‘bottom- up’ approach of building materials only the colloidal systems with particle dimensions less than 50 nm are generally of interest [20].

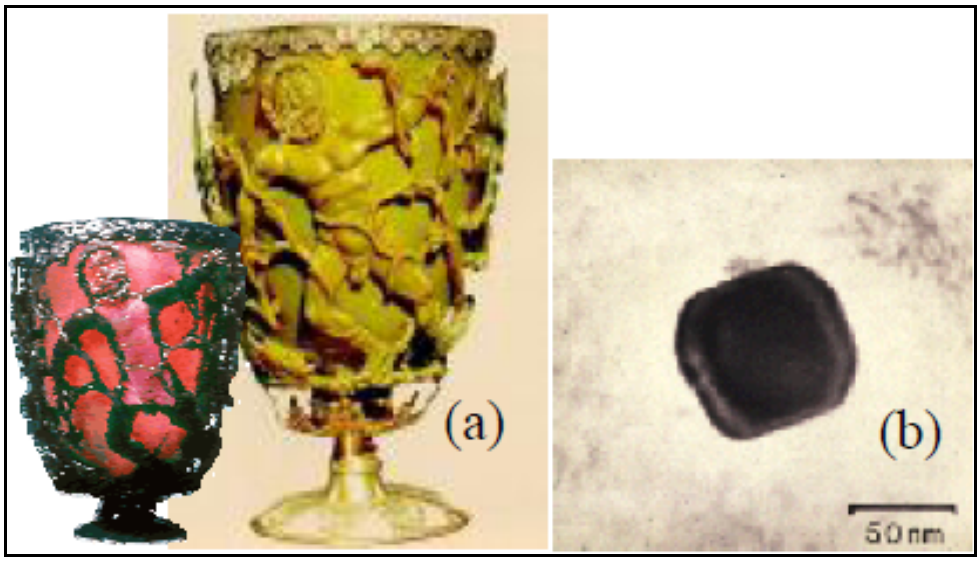

Figure 2.2. a. Lycurgus Cup, Roman Era (4th Century A.D). It appears green in reflected light and red in transmitted light. It contains gold and silver particles of approximately 70 nm, b. and in the ratio 1:14. The special color effect is due to these nanocrystals [20]

NPs show a number of properties that are either absent in or more efficient than their bulk materials counterparts. Some of the properties are due to quantum or more generally size effects, some are due to increased surface-to-volume ratio or shape some to the presence of an organic ligand shell, but some are more collective and derive from the assembly and arrangement of the NPs [21].

Synthesis and manipulation of clusters in this size range falls in the domain of nanotechnology and the clusters are often called as NPs. The emerging field of nanotechnology will require tailor made building blocks for the bottom-up construction of advanced materials and devices. The availability of colloidal particles with unique and tailored functional properties like optical, mechanical and electrical properties has made colloidal synthesis the favored method for obtaining NPs [20].

2.2. MAGNETIC NANOPARTICLES

Magnetic nanoparticles (MNPs) are a class of NPs which due to their magnetic properties can be manipulated using magnetic field. Such particles commonly consist of magnetic elements such as iron, nickel and cobalt and their chemical compounds [22].

Iron oxides exist in many forms in nature, with magnetite (Fe_3O_4), maghemite (γ-Fe_2O_3), and hematite (α-Fe_2O_3) being probably the most common. These three oxides are also very important technologically. However, in MNP applications, magnetite, Fe_3O_4, is the mostly promising form of all, due to its biocompatibility, high superparamagnetic properties and high magnetic susceptibility [23]. Some of their physical and magnetic properties are summarized in Table 2.1.

Hematite is the oldest known of the iron oxides and is widespread in rocks and soils. It is also known as ferric oxide, iron sesquioxide, red ochre, specularite, specular iron ore, kidney ore or martite. Hematite is blood-red in color if finely divided, and black or grey if coarsely crystalline. It is extremely stable at ambient conditions, and often is the end product of the transformation of other iron oxides. Magnetite is also known as black iron oxide, magnetic iron ore, loadstone, ferrous ferrite, or Hercules stone. It exhibits the

strongest magnetism of any transition metal oxide. Maghemite occurs in soils as a weathering product of magnetite, or as a product of heating of other iron oxides [23].

Table 2.1. Physical and magnetic properties of iron oxides [23]

Property	**Hematite**	**Magnetite**	**Maghemite**
Molecular Formula	α-Fe_2O_3	Fe_3O_4	γ-Fe_2O_3
Density (g/cm^3)	5.26	5.18	4.87
Melting point (°C)	1350	1583-1597	-
Type of magnetism	Weakly ferromagnetic or antiferromagnetic	Ferromagnetic	Ferrimagnetic

The crystal structure of the three iron oxides can be described in terms of close-packed planes of oxygen anions with iron cations in octahedral or tetrahedral interstitial sites. In hematite, oxygen ions are in a hexagonal close-packed arrangement, with Fe(III) ions occupying octahedral sites (Figure 2.3. (a)). In magnetite and maghemite, the oxygen ions are in a cubic close-packed arrangement (Figure 2.3.(b)). Magnetite has an inverse spinel structure with Fe(III) ions distributed randomly between octahedral and tetrahedral sites, and Fe(II) ions in octahedral sites. Maghemite has a spinel structure that is similar to that of magnetite but with vacancies in the cation sublattice [23].

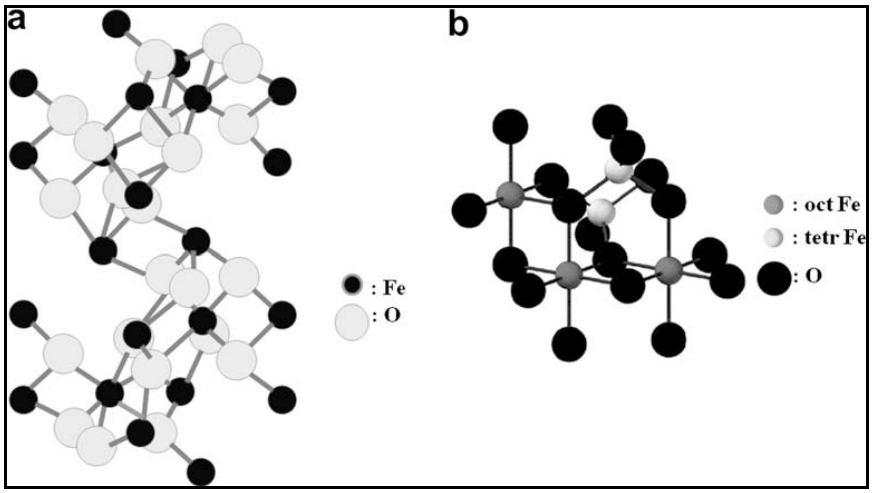

Figure 2.3. Crystal structures of a. hematite, b. magnetite [23]

2.2.1. Superparamagnetism

Nanosized magnetic particles have physical and chemical properties that are characteristic of neither the atom nor the bulk counterparts. Quantum size effect and the large surface area of MNPs dramatically change some of the magnetic properties and exhibit superparamagnetic phenomena and quantum tunnelling of magnetization, because each particle can be considered as a single magnetic domain [24].

MNPs have a novel response in the presence of magnetic fields. Figure 2.4 shows the response of MNPs in a magnetic fluid in the presence of magnetic field [25].

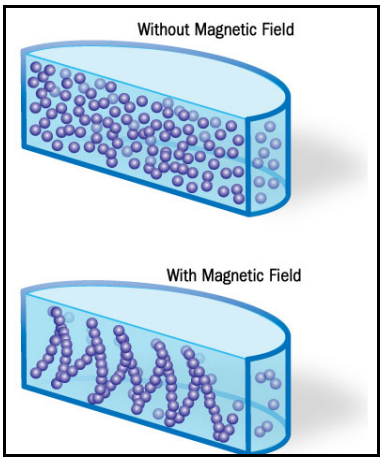

Figure 2.4. The response of MNPs to the presence and absence of magnetic field [25]

Superparamagnetism occurs when the material is composed of very small crystallites (1–10 nm). It is a phenomenon by which magnetic materials may exhibit a behavior similar to paramagnetism even when at temperatures below the Curie or the Néel temperature [26]. The Curie and Néel temperature are the temperatures at which a magnetic material becomes paramagnetic [27]. This is a small length-scale phenomenon, where the energy required to change the direction of the magnetic moment of a particle is comparable to the ambient thermal energy. At this point, the rate at which the particles will randomly reverse direction becomes significant [26].

Normally, coupling forces in ferromagnetic materials cause the magnetic moments of neighboring atoms to align, resulting in very large internal magnetic fields (Figure 2.5). This distinguishes ferromagnetic materials from paramagnetic materials. At temperatures above the Neel temperature, the thermal energy is sufficient to overcome the coupling forces, causing the atomic magnetic moments to fluctuate randomly. Because there is no longer any magnetic order, the internal magnetic field no longer exists and the material exhibits paramagnetic behavior [26].

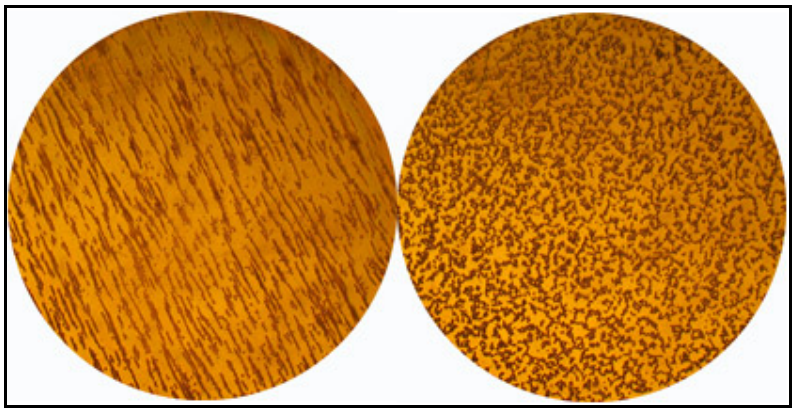

Figure 2.5. Superparamagnetic particles a. under the influence of an external magnetic field, b. in absence of an external magnetic field, monodisperse particle distribution [26]

2.2.2. Synthesis Methods

One of the latest tendencies in materials science is to tailor make classical products with controlled properties for special uses. Particular attention should be paid to the preparation methods that allow the synthesis of particles nearly of uniform size and shape. This goal can be achieved by precipitation from a homogeneous solution under controlled conditions or by controlling the particle growth in a process where a precursor in aerosol or vapor form is decomposed. Examples of such preparations include gold colloids, sulfur sols, metal oxides and hydrous oxides [28].

Many wet chemical routes have been developed in recent years. Synthesis of monometallic magnetic particles such as Fe, Co or Ni have been successfully done by electrochemical reduction, chemical reduction by Li, hydroborides, or polyols of metal salts, thermal decomposition in organic solvents in the presence of bulky stabilizers such as: i) fatty acids (in combination with organic amines or phosphanes); ii) polymers, or; iii) surfactants [29]. Surfactant is an abbreviation of "Surface active agent". They are usually organic compounds that are amphiphilic, meaning they contain both hydrophobic groups (their "tails") and hydrophilic groups (their "heads"). Therefore, they are typically sparingly soluble in both organic solvents and water. Surfactants coat the surface of the nanoparticle, therefore stop their further growing thus stabilizing the particles and preventing their further agglomeration [30].

The three most common approaches used to produce MNPs are physical vapor deposition, mechanical attrition, and chemical routes from solution. In both the vapor phase and solution routes, the particles are assembled from individual atoms to form NPs. Alternatively, mechanical attrition involves the fracturing of larger coarse-grained materials to form nanostructures [29].

The most common preparation of magnetite (Fe_3O_4) ferrofluids was developed by Massart about 20 years ago and described in detail in 1987. The synthesis was based on the co-precipitation of Fe^{II} and Fe^{III} salts in aqueous solutions stabilized by repulsive electrostatic forces. TEM investigations show typically aggregated particles, consisting usually of a mixture of ferrimagnetic magnetite, and maghemite (γ-Fe_2O_3), and paramagnetic hematite (α-Fe_2O_3). The ratio of the different iron oxide phases is directly compared to the expense associated with performing the synthesis under oxygen free conditions, because γ-Fe_2O_3 and α-Fe_2O_3 are oxidation products of Fe_3O_4 [29].

Additionally, many reports dealt with solving the classic problem of NP aggregation in aqueous solutions. To overcome such aggregation, new preparations have involved micellar solutions, as well as the transfer of iron oxide particles from aqueous to nonpolar solvents by hydrophobizing the surface by adsorbing bulky stabilizers such as fatty acids [29].

Different methods have been applied to decrease particle size distribution. One method that has been successfully applied involves synthesis of iron oxides in reverse micelles. A second method dealt with a size selective precipitation after transfer of iron oxide particles to nonpolar organic solvents. Sun et al. have developed a very successful method to achieve monodisperse Fe_3O_4 NPs without a size selection procedure. This method is based on the reduction of iron(III) acetylacetonate by 1,2-hexadecanediol and further thermal decomposition at high temperatures (solvent: diphenyl ether, b.p. 265°C) in the presence of oleic acid and oleylamine as stabilizers. As a result, small Fe_3O_4 NPs are formed and can be further grown by seed-mediated growth [31].

2.2.3. Applications of MNPs

MNPs have emerged as an important building block in nanobiotechnology since they can be obtained in sizes comparable to those of a protein, antibody, DNA or RNA, and can interact with or bind to such biomolecules. Their magnetic properties lead to magnetic carriers for biomedical applications such as DNA and RNA purification, cell separation, magnetic drug delivery, hyperthermia and magnetic resonance imaging (MRI) contrast enhancement [4-7].

Cell labelling with ferro/paramagnetic substances is an increasingly common method for in vivo cell separation as the labelled cells can be detected by Magnetic Resonance Imaging (MRI) [24].

Superparamagnetic iron oxide NPs also play an important role as MRI contrast agents, to better differentiate healthy and pathological tissues. Recent developments in MRI have enabled in vivo imaging at near microscopic resolution]. In order to visualize cells by MRI, it is necessary to tag cells magnetically [24].

Tissue repairing is another application by using MNPs. Tissue repair using iron oxide NPs is accomplished either through welding, apposing two tissue surfaces then heating the tissues sufficiently to join them, or through soldering, where protein or synthetic polymer-coated NPs are placed between two tissue surfaces to enhance joining of the tissues. NPs that strongly absorb light corresponding to the output of a laser are also useful for tissue-repairing procedures. Specifically, gold- or silica-coated iron oxide NPs has been designed to strongly absorb light. The NPs are coated onto the surfaces of two pieces of tissue at the site where joining was desired. This technique affords methods to minimize tissue damage by using the least harmful wavelengths of light and/or lower powered light sources [24].

Another possible and most promising application of these colloidal MNPs is in drug delivery as carriers of drug for site-specific delivery of drugs. Ideally, they could bear on their surface or in their bulk a pharmaceutical drug that could be driven to the target organ and released there. For these applications, the size, charge and surface chemistry of the magnetic particles are particularly important and strongly affect both the blood circulation

time as well as bioavailability of the particles within the body. In addition, magnetic properties and internalization of particles depend strongly on the size of the magnetic particles [24].

Magnetic induction hyperthermia, one of the therapies for cancer treatment, means the exposition of cancer tissues to an alternating magnetic field. Magnetic field is not absorbed by the living tissues and can be applied to deep region in the living body. When magnetic particles are subjected to a variable magnetic field, some heat is generated due to magnetic hysteresis loss. The amount of heat generated depends on the nature of magnetic material and of magnetic field parameters. Magnetic particles embedded around a tumor site and placed within an oscillating magnetic field will heat up to a temperature dependent on the magnetic properties of the material, the strength of the magnetic field and the frequency of oscillation and the cooling capacity of the blood flow in the tumor site. Cancer cells are destroyed at temperature higher than 43 °C, whereas the normal cells can survive at higher temperatures [24].

2.3. GOLD COATED MNPs (CORE/SHELL)

Core/shell NPs are nanostructures that have core made of a material coated with another material [32]. An example of core/shell structure can be seen from Figure 2.6. The necessity to shift to core/shell NPs is the improvement in the properties. Some examples for the properties are given in the Figure 2.7 [33]. Taking into consideration the size of the NPs, the shell material can be chosen such that the agglomeration of particle can be prevented. This implies that the monodispersity of the particles can be improved. The core/shell structure enhances the thermal and chemical stability of the NPs, improves solubility, makes them less cytotoxic and allows conjugation of other molecules to these particles. The shell can also prevent the oxidation of the core material [34].

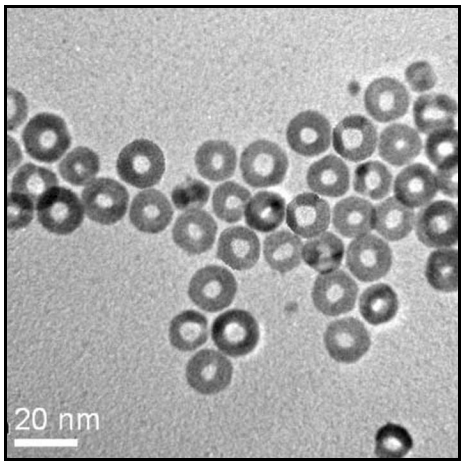

Figure 2.6. Ag/Au core/shell NPs [32]

The range of biomedical applications of MNPs depends on their stability in solutions at various pHs and the degree to which their surfaces may be chemically functionalized. Surface modifications of MNPs with different stabilizers including organic and inorganic molecules affect their stability, magnetization and, therefore, biomedical applications. Specific coating methods of chemical modifiers and their subsequent geometric arrangement on the NPs determine not only the overall size of the resulting colloid but also play a key role in the biokinetics and biodistribution of NPs in the body. Many researchers have successfully modified the gold surface of NPs with a variety of alkenethiols that can be further modified with biological molecules [35].

Microemulsion methods have been used extensively for the fabrication of structures containing silica or gold shells and monometallic Fe or Fe oxide particles. Pure Fe core NPs that were successfully fabricated by many methods demonstrated good properties for biological applications [35]. Carpenter prepared metallic iron particles coated by a thin layer of gold via a microemulsion. The gold shell protects the iron core against oxidation and also provides functionality, making these composites applicable in biomedicine [24].

Zhou *et al.* prepared gold coated iron core-shell structure NPs (Fe/Au), synthesized using reverse micelles characterized by transmission electron microscopy (TEM). The average NP size of the core-shell structure is about 8 nm, with about 6nm diameter core and 1–2 nm shell. The magnetic measurement of the NPs also proved successful synthesis

of gold-coated iron core/shell structure. The NPs were then assembled under 0.5 T magnetic field and formed parallel nanobands about 10 mm long [24].

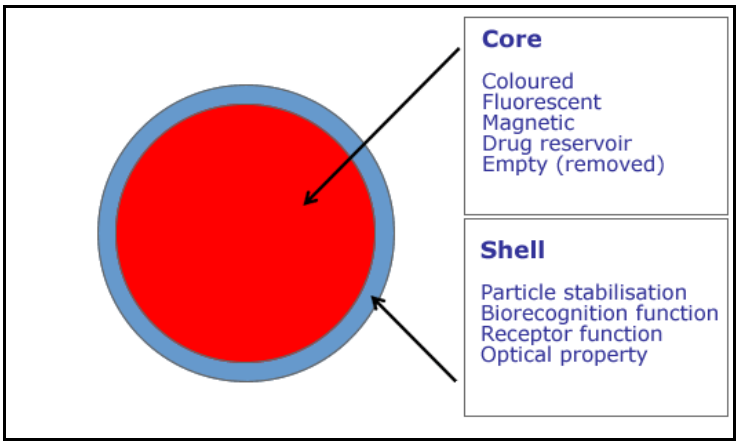

Figure 2.7. Effect of shell on properties of NPs [33]

Core/shell NPs comprise a core of one material and a coating shell of another material. The composition of the core and shell can be varied to give a wide range of different properties which are described in Figure 2.7 [33].

2.4. SELF ASSEMBLY

As mentioned in the Section 2.1 there are two different approaches in assembly of nanostructures. These are top-down approach and bottom-up approach. Since Paleolithic age, people use top-down approach in industry and many other fields. In top-down approaches, big particles are minimized into smaller scales in order to be used for further steps. On the other hand, in bottom-up approaches, small particles are obtained or synthesized and used to build higher structures, Figure 2.1 shows the difference of bottom-up and top-down approaches. The bottom-up approach that was introduced in Feynman's speech in 1959, is being used nowadays especially in preparing nanostructured surfaces. Lithography and micro contact printing techniques are the examples of top-down approach used in nanostructured surface preparation studies [36, 37]. Since those techniques are troublesome and expensive, usage of nanostructures in bottom-up approach based techniques have been emerged. The NPs' surface properties play influential role in bottom

up approach based techniques. The surface chemistry determines the solution properties that the NPs are suspended in. The surface property of the NP is determined by the synthesis method or it can be altered with a chemical attachment or physical adsorption of wanted molecules [38-41].

The process of NP self-assembly on surfaces is controlled by the surface properties of the NPs, the nature of the substrate, the NP dispersion from which the self-assembly occurs and the method of deposition. There are several factors, which can determine the quality of the final self-assembled structure. These factors include particle size, particle size distribution, surfactant chain length, and the conditions of deposition. Some of the important technical challenges to the preparation of well-defined, self-assembled monolayers of NPs lie in the synthesis method and the choice of surfactant coating on the NPs. Varying the concentration of the surfactant in the solution used to wash the NPs after their synthesis has no effect on the size of the NPs but effects the self-assembly of the particles from dispersions evaporated, dip-coated or spin-coated onto substrate surfaces.

Most of the NPs self-assemble in the solutions or suspensions on any solid surfaces, upon evaporation of the solvent of droplet. During the drying of the droplets, some physical, chemical or magnetic forces can be applied on.

The self assembly from a drying droplet occurs because as the solvent is evaporated from the droplet of suspension, the weak forces become dominant among the NPs. Before the evaporation process starts, the particles disperse well in the suspension. The evaporation process occurs on the surface of the droplet. As the droplet starts to evaporate, the concentration increases. The reason for self-assembly of NPs during evaporation process lies on the fact that the evaporation of solvent is faster than the diffusion rate of NP during this increase of concentration.

This phenomenon was reported by Denkov and coworkers. They explained the driving mechanism for the formation of irreversible packing NPs by thermodynamics of non-equilibrium processes of aggregating NPs [42, 43]. By using this method, easy, simple and cheap way of preparing nanostructured surfaces can be achieved. Several surfaces can

be obtained by using gold, silver or polystyrene NPs. Furthermore, using various morphologies of NPs and NPs in various solvents may result obtaining diverse surfaces.

To sum up, in order to fulfill the aim since the Fe_3O_4 is the most promising iron oxide, due to its biocompatibility, high superparamagnetic properties and high magnetic susceptibility, it was used as the MNP for this study. These particles are also coated with gold to enhance its chemical interness and biocompatibility. It is clear from the literature that there is a need for a facile method to control the self-assembly of NPs (magnetic or gold-coated magnetic in this case) on surfaces, which we tried to address with this work.

3. MATERIALS AND METHODS

In this chapter, the chemicals that were used during the synthesis of both hydrophilic and hydrophobic MNPs are given. Those hydrophobic ones were further used to synthesize gold coated MNPs therefore, the chemicals belong to the gold coating process are also tabulated. Furthermore, the methods which were used to characterize the synthesized NPs are also included.

3.1. CHEMICALS

Table 3.1. Chemicals for synthesis of hydrophobic MNPs

Chemical name	Formula	Provider	Purity
Ferric Acetylacetonate	$C_{15}H_{21}FeO_6$	Fluka	97%
1,2 – Tetradecanediol	$CH_3(CH_2)_{11}CH(OH)CH_2OH$	Aldrich	90%
Oleic Acid	$C_{18}H_{34}O_2$	Riedel-de Haen	99%
Oleylamine	$C_{18}H_{37}N$	Fluka	70%
Dibenzylether	$C_{14}H_{34}O_2$	Merck	Pure

Table 3.2. Chemicals for synthesis of hydrophilic MNPs

Chemical name	Formula	Provider	Purity
Iron (II) sulfate hepta hydrate	$FeSO_4.7H_2O$	Riedel-de Haen	90%
Iron (III) Chloride	$FeCl_3$	Riedel-de Haen	97%
Capric Acid	$C_{10}H_{20}O_2$	Fluka	98%
Ammonium Hydroxide	NH_4OH	Riedel-de Haen	99%
Water	H_2O	-	-

Table 3.3. Chemicals for synthesis of gold coated hydrophobic MNPs

Chemical name	**Formula**	**Provider**	**Purity**
Gold Acetate	$Au(O_2CCH_3)_3$	Alfa-Aesar	99.9%
1,2 – Tetradecanediol	$CH_3(CH_2)_{11}CH(OH)CH_2OH$	Aldrich	90%
Oleic Acid	$C_{18}H_{34}O_2$	Riedel-de Haen	99%
Oleylamine	$C_{18}H_{37}N$	Fluka	70%
Dibenzylether	$C_{14}H_{34}O_2$	Merck	Pure

Table 3.4. Chemicals used as solvents

Chemical name	**Formula**	**Provider**	**Purity**
Hexane	C_6H_{14}	Riedel-de Haen	95%
Heptane	C_7H_{16}	Lab-Scan	95%
Decane	C_8H_{18}	Riedel-de Haen	95%

Table 3.5. Chemicals used for iron test

Chemical name	**Formula**	**Provider**	**Purity**
Tiron	$C_6H_{14}Na_2O_8S_2$	Riedel-de Haen	98.5%
Hydrochloric Acid	HCl	Merck	98.5%
Sodium Hydroxide	NaOH	Fluka	99%

Table 3.6. Chemicals for synthesis of hydrophilic MNPs from hydrophobic particles

Chemical name	**Formula**	**Provider**	**Purity**
1,2 Dicholorobenzene	$C_6H_{14}Cl_2$	Riedel-de Haen	98%
N,N-dimethyl formamide	C_3H_7NO	Sigma Adrich	98%
Citric Acid	$C_6H_8O_7$	Sigma Adrich	99%

3.2. CHEMICALS AND MATERIALS FOR TEMPLATE PREPARATION

Compact disc (CD) with the brand Princo, PDMS (Poly(dimethyl siloxane)) which was purchased from Dow Corning in USA and Magnetic Beads (MBs) from AdemTech in France were used by Deniz Sandal who was a MSc student of the Genetics and Bioengineering Department in Yeditepe University in order to prepare the template for the patterning part of the work.

The purchased MBs were two types: amine functionalized (MB-a) and carboxyl functionalized (MB-c). Table 3.7 shows the properties of MBs. The MBs were mono dispersed and superparamagnetic beads. They were composed of magnetic core encapsulated by a hydrophilic polymer shell as it is schematically shown in the Figure 3.1. The surface of bead was activated with amine or carboxylic acid functionality.

Table 3.7. The properties of the MBs

	MB-a	MB-c
Mean diameter (nm)	510±20	510±20
Weight per cent	1.0±0.1	5.0±0.1
Solid content (mg/mL)	10	50
Particle number (per mL)	6.02×10^{10}	3.6×10^{11}
Specific surface area (m^2/g)	5	5
Fe_3O_4 content (per cent)	70	70
Magnetization at saturation (emu/g)	40	40

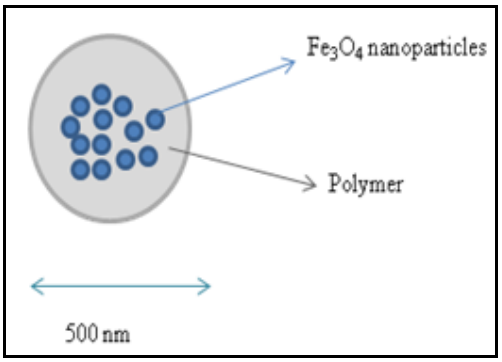

Figure 3.1. MBs

3.3. CHARACTERIZATION METHODS

3.3.1. Dynamic Light Scattering (DLS)

Dynamic Light Scattering is a technique which can be used to determine the particle size distribution over a range of 1 nm to 6 μm. The particle size of a powder, granular material or particles dispersed in fluid is a list of values or mathematical function that defines the relative amounts of particles present, sorted according to size. It detects the fluctuations of the scattering intensity due to the Brownian motion of molecules in solution. Analysis of these intensity fluctuations yields the velocity of the Brownian motion and hence the particle size using the Stokes-Einstein relationship [44].

$$D = \frac{K_B T}{3\pi\mu d_H} \tag{3.1}$$

The hydrodynamic diameter (d_H) which is the size of a sphere that has the same diffusion behavior. The only parameters required in the Equation 3.1 are the absolute temperature T, the universal Boltzmann constant K_B, and the viscosity μ of the medium. In practice, the main parameters of interest, when performing DLS experiments, are the temperature, the refractive index and the viscosity [44].

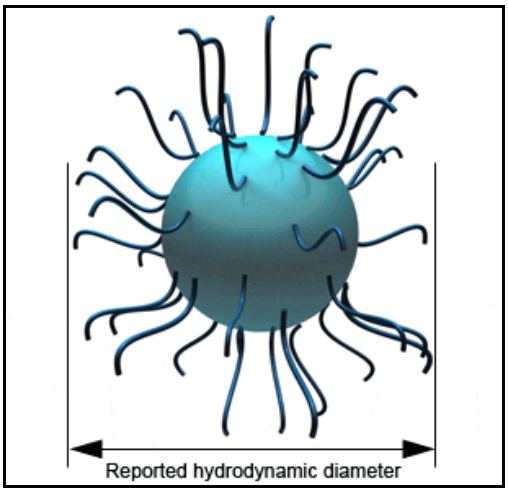

Figure 3.2. Hydrodynamic diameter measure by DLS [44]

The only requirement for this technique is enough light must be scattered to achieve sufficient statistical accuracy of the correlation function. In most instruments a He-Ne laser with a fixed wavelength of 633 nm is used as the light source which focuses on the particle dispersion by the help of the focusing lens. Light is scattered by the particles at all angles. However a dynamic light scattering instrument typically uses one detector thus detects scattered light at one angle which is 90^{o}. The intensity fluctuations of the scattered light are converted into electrical pulses which are fed into a data correlation yielding the appropriate data [44].

During the size analysis of the magnetite nanofluids, Malvern Zatasizer Nano series was used.

3.3.2 X-Ray Diffraction (XRD)

X-ray diffraction (XRD) is a versatile, non-destructive technique that reveals detailed information about the chemical composition and crystallographic structure of natural and manufactured materials [45].

Radiations striking a material may be scattered or absorbed. X-rays, high energy electrons and neutrons are used to extract structural information of crystal lattice. Incident

radiations of sufficiently smaller wavelength interact elastically with the regular array of atoms in a crystal lattice to yield a diffraction pattern. Both diffraction angles and the intensities in various diffracted beams are sensitive function of crystalline structure. The diffracted angles depend on the Bravais point lattice and unit cell dimensions, while the diffracted intensities depend on the atomic numbers of the constituent atoms and their geometrical relationship with respect to the lattice points. The condition for a crystalline material to yield a discrete diffraction pattern is that the wavelength of incident radiation should be comparable to or less than the interatomic spacing in the lattice. A convenient form of the geometrical relationship determining the angular distribution of the peak intensities in the diffraction pattern from a regular crystal lattice is the Bragg's equation [46].

$$n\lambda = 2d \sin \theta \tag{3.2}$$

Where n is an integer referring to the order of reflection, λ is the wavelength of the radiation, d is the spacing between the crystal lattice planes responsible for a particular diffracted beam and θ is the angle that incident beam makes with lattice planes [46].

The X-Ray detector moves around the sample and measures the intensity and the position of the peaks. The highest peak is defined as the 100% peak and the intensity of all the other peaks are measured as a percentage of the 100% peak [46].

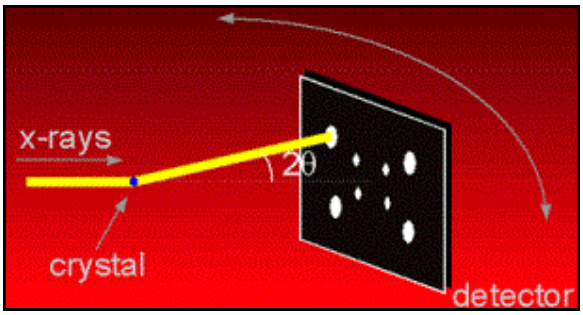

Figure 3.3. X-ray diffraction [46]

The synthesized NPs were also characterize by using the XRD (Rigaku D/MAX-Ultima+/PC) whether they give the characteristic patterns of the desired crystal.

3.3.3. Transmission Electron Microscope (TEM)

A transmission electron microscope (TEM) a microscopy technique whereby a beam of electrons is transmitted through an ultra thin specimen, interacting with the specimen as it passes through. An image is formed from the interaction of the electrons transmitted through the specimen; the image is magnified and focused onto an imaging device [47].

TEM operates on the same basic principles as the light microscope but uses electrons instead of light. Since wavelength of electrons is much lower than the light, TEMs are capable of imaging at a significantly higher resolution than light microscopes [47].

Objects to the order of a few angstroms (10^{-10} m) can be seen with this microscope. For example, small details in the cell or different materials can be studied down to near atomic levels. The possibility for high magnifications has made the TEM a valuable tool in both medical, biological and materials research [47].

A "light source" at the top of the microscope emits the electrons that travel through vacuum in the column of the microscope. Instead of glass lenses focusing the light in the light microscope, the TEM uses electromagnetic lenses to focus the electrons into a very thin beam. The electron beam then travels through the specimen that is studied. Depending on the density of the material present, some of the electrons are scattered and disappear from the beam. At the bottom of the microscope the unscattered electrons hit a fluorescent screen, which gives rise to a "shadow image" of the specimen with its different parts displayed in varied darkness according to their density. The image can be studied directly by the operator or photographed with a camera [48].

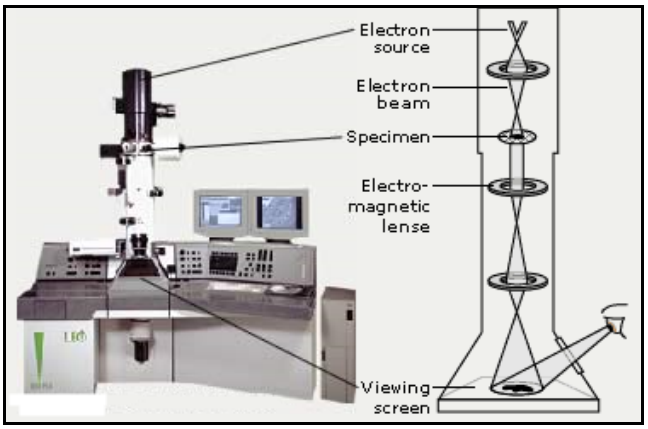

Figure 3.4. Individual parts of a typical TEM [48]

In this work, TEM (Model: Tecnai G2 F30) was used to characterize the synthesized magnetite and gold coated magnetite NPs.

3.3.4. Scanning Electron Microscope (SEM)

Scanning electron microscope (SEM) uses electrons instead of light or a probe to form an image. Since SEM has many advantages over traditional microscope as having large depth of field, higher resolution, controlling the degree of magnification [49]. The SEM gives information about microscopic details of the surface of the specimen in 1D. A sample that will be studied by using SEM should be conductive. Therefore, by using coating device, a thin gold layer is usually coated on the top of the sample. The gold layer-coating helps to obtain better images. In SEM, electron gun sends extremely focused beam of electrons towards to the specimen surface. The SEM image is formed by the signal of the reflected electrons. It presents intense images where zero signals are displayed as black, intermediate signals as shades of grey and maximum signal as white. The SEM uses the backscattered or emitted electrons from the specimen surface [50]. Figure 2.8 shows a cartoon view of SEM.

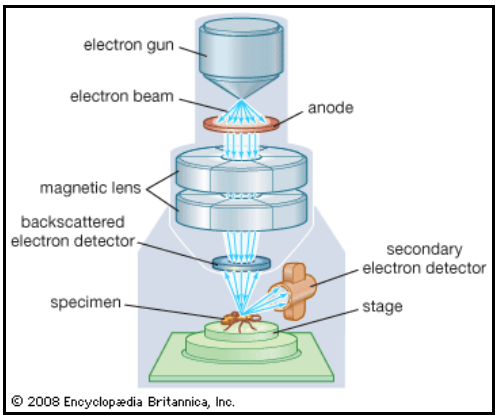

Figure 3.5. The schematic illustration of SEM [50]

The resolution obtained by using light microscope is approximately higher than 200 nm (wavelength of green light= 500 nm) with magnifications up to 3000 times. On the other hand, SEM provides resolution of less than 5 nm (wavelength of 30 kV electrons=0.007 nm) with magnifications up to 1 million times [50]. In Figure 3.6, the comparison of light microscope and EM can be observed.

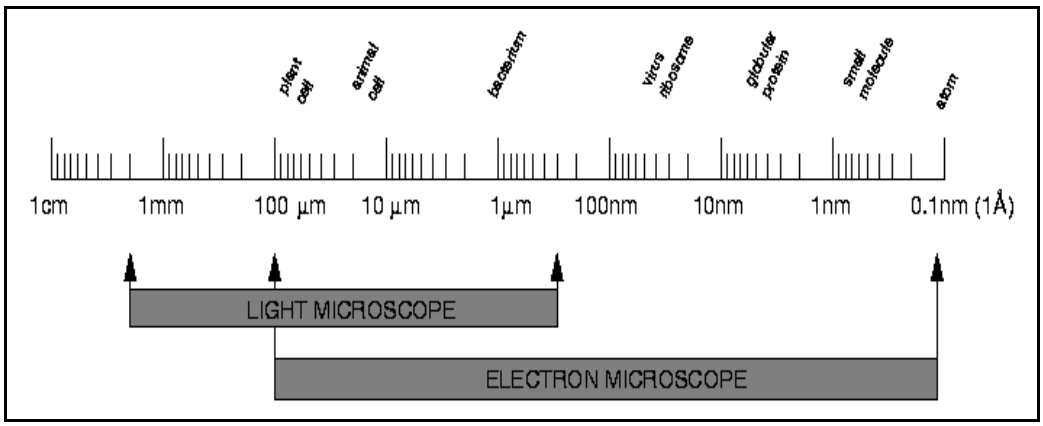

Figure 3.6. The visible region for EMs and light microscopes [51]

In this research work, SEM (XL30 ESEM-FEG/EDAX system) was used to observe the pattern formation on flat surfaces.

4. SYNTHESIS AND CHARACTERIZATION OF MNPs

In this chapter, different synthesis techniques of both hydrophilic and hydrophobic MNPs as well as gold coating process are given. Determination of the concentration of MNPs suspended in oil and water is also included. Finally the characterization of the synthesized particles is illustrated by using DLS, XRD and TEM results..

4.1. SYNTHESIS OF HYDROPHOBIC MNPs

In the synthesis of hydrophobic MNPs, the aim is to obtain 6.5 – 7 nm NPs in diameter. More than one surfactant were used such as Oleic acid, Oleylamine and 1,2 Tetradecanediol in order to have an efficient and stable magnetic fluid.

In this synthesis method, very high temperatures were reached (up to 300 ^{o}C) which resulted in the formation of MNPs of approximately 6 to 11 nm depending on the rate of the temperature increase. For a rate of 2.5 ^{o}C/min, 6 nm of NPs were obtained while 5 ^{o}C/min approximately yielded 11 nm of MNPs.

The organic-phase synthesis of magnetite was described previously [31] and this procedure was used with minor modifications. In a typical synthesis, Iron (III) acetylacetonate (0.706 g), 1,2-Tetradecanediol (2.3039 g), Oleic acid (1.9 mL), Oleylamine (1.69 mL) and Dibenzyl ether (20 mL) were mixed under magnetic stirring in N_2 environment. After mixing the needed chemicals in a round bottom flask, under constant magnetic stirring, the sample was heated up to 100 ^{o}C. When the desired temperature was reached the solution was kept at that temperature for 15 minutes. Then the solution was again heated up to 200 ^{o}C with pre-decided rate of temperature increase but at 180 ^{o}C, nitrogen blanket was done in order to apply pressure on the reaction mixture which allowed the solutions to reach higher temperatures without any reflux taking place. The remaining steps of the experiment were carried out under nitrogen blanket. After reaching 200 ^{o}C, the reaction mixture was kept at that temperature for 2 hours and then again heated up to 300 ^{o}C with the same rate of temperature increase. Particles were precipitated upon

addition of methanol and separated by centrifugation followed by drying in a vacuum oven. Particles were then suspended in the desired organic solvent.

Experimental set-up for synthesis of hydrophobic MNPs is given in Figure 4.1, consists of automated heater (1), nitrogen blanket (2), mercury (3), thermo-couple for temperature control (4) and the reaction mixture in closed round bottom flask (5).

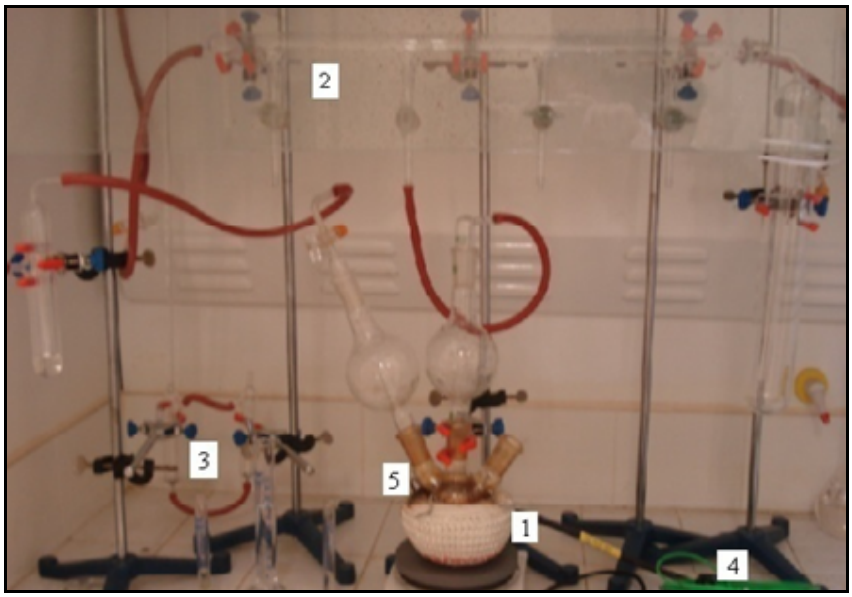

Figure 4.1. Experimental set-up for synthesis of hydrophobic MNPs

4.2. SYNTHESIS OF GOLD COATED HYDROPHOBIC MNPs

The synthesis procedure was taken from Chung *et al* [52] and used with minor modifications. 0.1 g of the synthesized hydrophobic magnetite was dispersed in dibenzylether. To the suspension 2.2 mmol Gold acetate , 12 mmol 1,2 – Tetradecanediol, 0.5 mL Oleic acid and 3 mL Oleylamine were added and mixed under magnetic stirring in N_2 environment. After mixing the needed chemicals in a round bottom flask, under constant magnetic stirring, the sample was heated up to 190 ^{o}C but at 180 ^{o}C, nitrogen blanket was done. The heating rate was the same as the synthesis of the magnetite (2.5 °C). After reaching 190 ^{o}C, the reaction mixture was kept at that temperature for 1 hour. Particles were precipitated upon addition of methanol and separated by centrifugation

followed by drying in a vacuum oven. Particles were then suspended in the desired organic solvent. Experimental set-up for synthesis is the same with the magnetite synthesis.

4.3. SYNTHESIS OF GOLD COATED HYDROPHOBIC MNPs

In a typical synthesis of hydrophilic MNPs (~ 8 nm), iron sulfate hepta-hydrate (2.412 g) and iron chloride (2.82 g) were solubilized in 80 mL of previously de-aerated water, for twenty minutes in a three neck round bottom flask. The de-aeration of water was done by passing nitrogen gas through the reaction medium. The reaction solution was heated up to 70 ^{o}C at a constant rate and at that temperature a solution of capric acid (2 g) in ammonium hydroxide (20 mL), where capric acid serves as a surfactant that stabilizes the MNPs from further growth and prevents agglomeration, was quickly added to the mixture and nitrogen gas which was used for de-aeration is disconnected. Upon this addition, blackening of the solution was immediately observed, indicating the formation of MNPs. The mixture was then heated up to 80 ^{o}C and was kept at that temperature for half an hour. After that, the mixture is allowed to cool down to room temperature.

The experimental setup shown in Figure 4.2 for synthesis of hydrophilic magnetite nanoparticles consists of automated heater (1), mechanical stirrer (2), closed round bottom flask (3), thermocouple (4), and nitrogen gas for de-aeration (5).

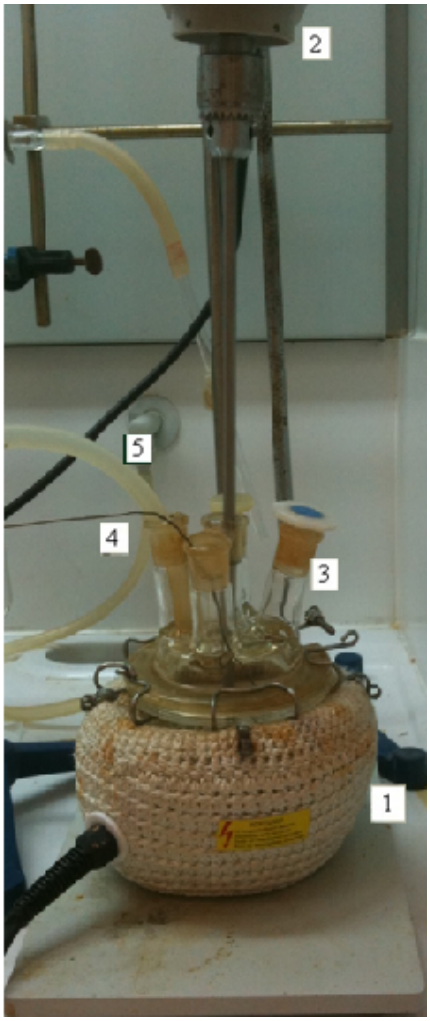

Figure 4.2. Experimental set-up for the synthesis of hydrophilic MNPs

4.4. IRON TEST FOR DETERMINING MAGNETITE CONCENTRATION

The magnetic property of a magnetic fluid originates from the magnetite core at the center of each NP. In order to quantify the amount of magnetite in magnetic fluids, a colorimetric iron analysis technique was developed. By this method, the Fe^{2+} and Fe^{3+} concentrations in solution can be determined, from which the total amount of magnetite in the fluid is calculated. The technique is mainly based on the ability of certain organic compounds to form complexes with the free iron ions in solution. The light absorption of formed iron complex at a certain wavelength is then measured by UV-VIS Spectrophotometry. The organic compound used for this colorimetric technique is 4,5-

dihydroxy-1,3-benzenedisulfonic acid, disodium salt, also known as Tiron reagent. This compound forms complexes with Fe^{2+} and Fe^{3+} ions in a ratio of three Tiron molecules to one iron molecule and shows an absorbance at 480 nm [53].

In a typical Tiron test, 0.1 mL of the concentrated magnetic nanofluid is taken and mixed with 0.4 mL of 37% concentrated HCl in a 25 mL volumetric flask to release the iron into solution as Fe^{2+} and Fe^{3+}. This solution is then heated under a heat gun at approximately 150^{o}C for a few seconds until the color of the solution turns to yellow. The hot acidic solution is left at room temperature to cool down and afterwards it is mixed with the proper amount of Tiron solution. After this step, 3 mL from 4 M of sodium hydroxide is added to the final solution to neutralize the acid. Upon the addition of the base, the color change to red is observed. The solution is then diluted using distilled water until the volume of the final solution reaches 25 mL.

The solution can be further diluted by the factor of 8-10 depending on the concentration of the final solution, so that it can be read by the UV-Spectrophotometer at 480 nm. The absorbance value is then inserted into the Equation 4.1 and the concentration is determined with the units of g/mL.

$$\text{Concentration}\left(\frac{g}{ml}\right) = \frac{(\text{ABS@480nm})x(\text{Dilution factor})x231.52x25}{39986x162.15x3x0.1} \quad (4.1)$$

In this equation 0.1 is the volume of the magnetic fluid, 3 is the iron ratio, 39986 is the extinction coefficient and 25 is the final volume of the solution which is further checked for the absorbance at 480 nm.

4.5. DISPERSING THE PARTICLES PREPARED BY OIL SYNTHESIS IN WATER

MNPs that are synthesized in oil can also be dispersed in water with performing another procedure which leads to the exchange of oil soluble surfactant on the surface with a water soluble surfactant. In this case obtained magnetite nanoparticles are dispersed in 1:1 mixture of 1,2 dichlorobenzene and N,N dimethylformamide in the presence of citric acid as indicated in Table 4.1 and the final solution is heated up to 100 ^{o}C with mechanical stirring. Solution is kept at that temperature for 24 hours. Upon completion of the reaction, the solution is mixed with ethyl ether for phase separation. By performing sufficient amount of centrifugation and phase separation, hydrophilic NPs can be obtained. In order to get rid of moisture, final product is left overnight in a vacuum oven at 60 ^{o}C.

By this method, more stable MNPs in water can be synthesized as compared to the previously mentioned synthesis carried out directly in water which is due to the direct chemical attachment of surfactant to the surface as opposed to a secondary layer self assembly.

Table 4.1. Conversion formulation for 480 mg of MNPs

Ingredients	**Amounts (g) or (ml)**
1,2 Dichlorobenzene	30
N,N Dimethylformamide	30
Citric Acid	0.4

4.6. CHARACTERIZATION OF MNPs

The synthesized magnetite nanoparticles by the methods given above were characterized in terms of their size, size distributions and crystallinity by transmission electron microscopy (TEM) technique dynamic light scattering (DLS) technique and x-ray diffraction (XRD), respectively.

4.6.1. Characterization of Hydrophobic MNPs

Hydrophobic MNPs synthesized by the above mentioned technique was characterized by TEM for their size. A typical TEM image is given in Figure 4.3. Based on the TEM images of synthesized magnetite, it can be concluded that the particle cores are spherical with approximately 6.1±2.1 nm in radius with a fairly narrow size distribution. DLS results show (Figure 4.4) the average hydrodynamic radius is measured to be 10.1±3.1, which is in perfect agreement with the TEM results where the stabilizing surfactant layer contributes to about 2 nm of thickness around the core.

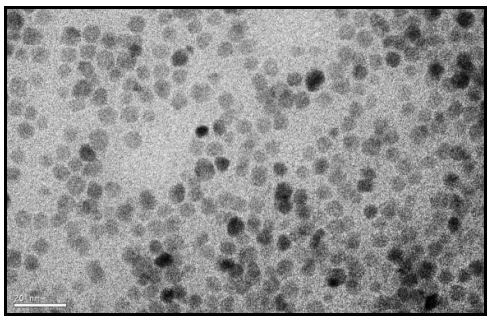

Figure 4.3. TEM image of hydrophobic MNPs

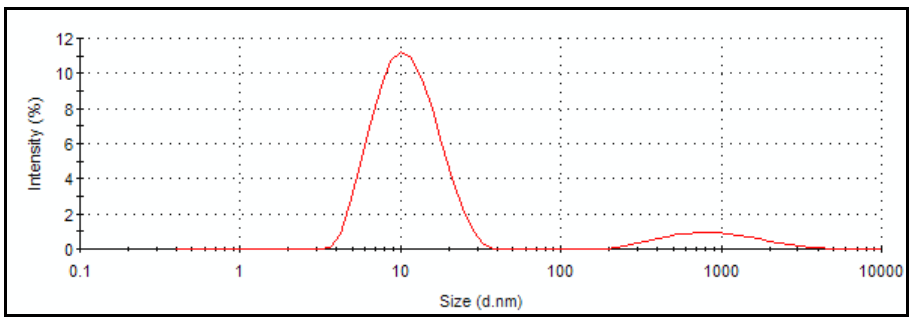

Figure 4.4. DLS data for hydrophobic synthesis of MNPs

Also, the XRD results exhibit the characteristic diffraction pattern of Fe_3O_4. Figure 4.5 shows the characteristic magnetite XRD peaks while Figure 4.6 shows the XRD graphs of synthesized hydrophobic MNPs.

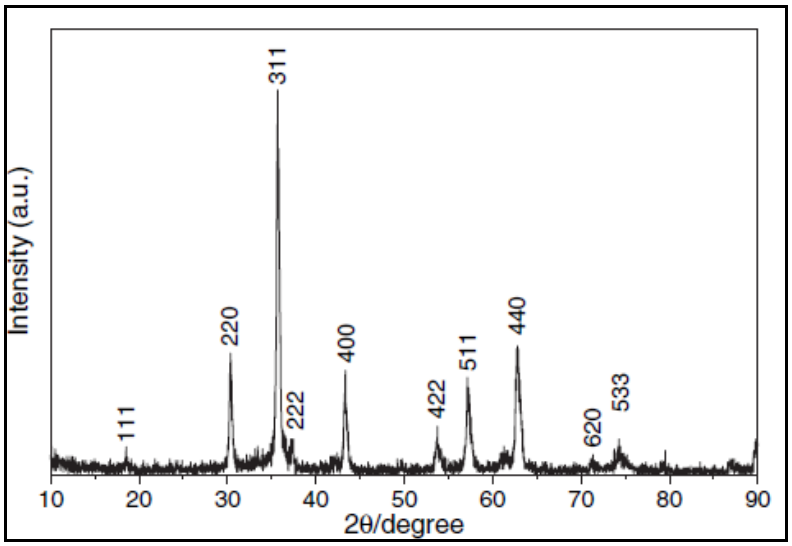

Figure 4.5. Characteristic XRD peaks of MNPs

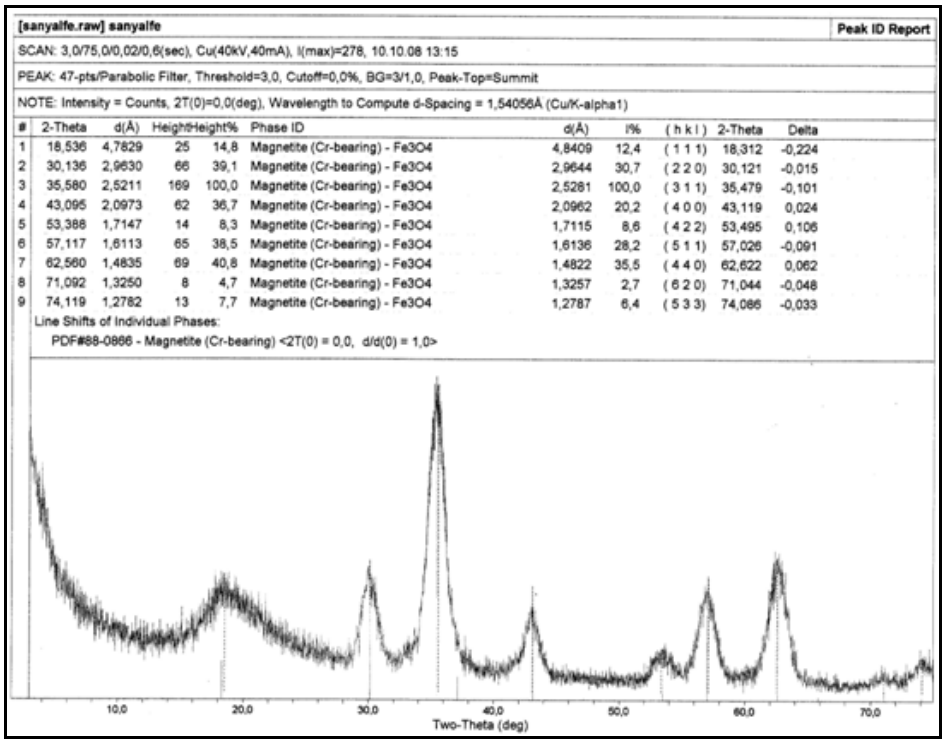
[sanyalfe.raw] sanyalfe — Peak ID Report

SCAN: 3,0/75,0/0,02/0,6(sec), Cu(40kV,40mA), I(max)=278, 10.10.08 13:15

PEAK: 47-pts/Parabolic Filter, Threshold=3,0, Cutoff=0,0%, BG=3/1,0, Peak-Top=Summit

NOTE: Intensity = Counts, 2T(0)=0,0(deg), Wavelength to Compute d-Spacing = 1,54056Å (Cu/K-alpha1)

#	2-Theta	d(Å)	Height	Height%	Phase ID	d(Å)	I%	(h k l)	2-Theta	Delta
1	18,536	4,7829	25	14,8	Magnetite (Cr-bearing) - Fe3O4	4,8409	12,4	(1 1 1)	18,312	-0,224
2	30,136	2,9630	66	39,1	Magnetite (Cr-bearing) - Fe3O4	2,9644	30,7	(2 2 0)	30,121	-0,015
3	35,580	2,5211	169	100,0	Magnetite (Cr-bearing) - Fe3O4	2,5281	100,0	(3 1 1)	35,479	-0,101
4	43,095	2,0973	62	36,7	Magnetite (Cr-bearing) - Fe3O4	2,0962	20,2	(4 0 0)	43,119	0,024
5	53,388	1,7147	14	8,3	Magnetite (Cr-bearing) - Fe3O4	1,7115	8,6	(4 2 2)	53,495	0,106
6	57,117	1,6113	65	38,5	Magnetite (Cr-bearing) - Fe3O4	1,6136	28,2	(5 1 1)	57,026	-0,091
7	62,560	1,4835	69	40,8	Magnetite (Cr-bearing) - Fe3O4	1,4822	35,5	(4 4 0)	62,622	0,062
8	71,092	1,3250	8	4,7	Magnetite (Cr-bearing) - Fe3O4	1,3257	2,7	(6 2 0)	71,044	-0,048
9	74,119	1,2782	13	7,7	Magnetite (Cr-bearing) - Fe3O4	1,2787	6,4	(5 3 3)	74,086	-0,033

Line Shifts of Individual Phases:

PDF#88-0866 - Magnetite (Cr-bearing) <2T(0) = 0,0, d/d(0) = 1,0>

Figure 4.6. XRD graph of hydrophobic MNPs

4.6.2. Characterization of Gold Coated Hydrophobic MNPs

Hydrophobic magnetite nanoparticles synthesized by the above mentioned technique was used as seed for gold coating procedure after characterization. When the gold coating applied, it was observed that the color of the hydrophobic MNPs turned into purple-brown color. The TEM images are given in the Figure 4.7, according to this image it can be said that after coating process the shape of the NPs are still spherical. Since the diffraction analysis could not been done, TEM images are not enough to characterize the synthesized particles.

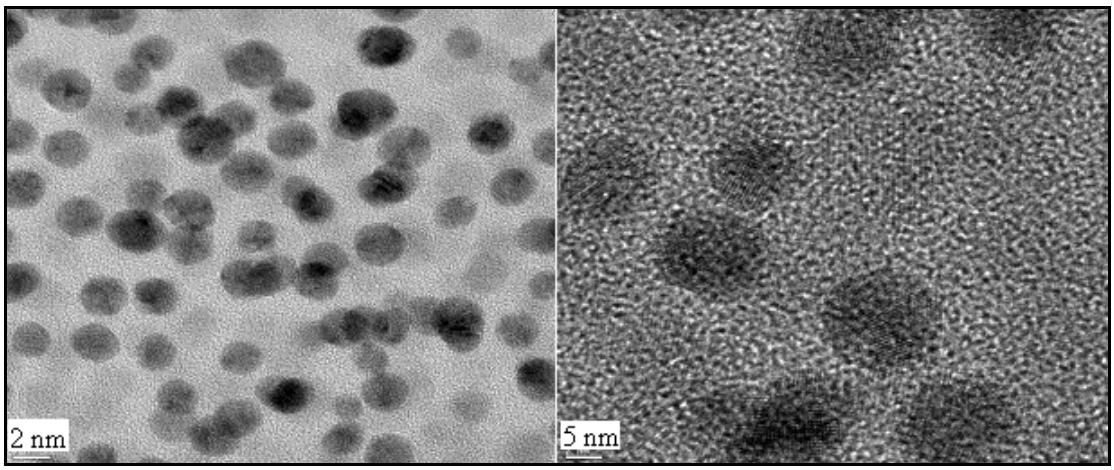

Figure 4.7. TEM images of gold coated hydrophobic MNPs

Since the refractive characteristics of gold is different from magnetite nanoparticles, XRD is the most important technique to show whether the surface of magnetite is covered by gold or not. Figure 4.8 shows the XRD graph of gold coated magnetite nanoparticles while the Figure 4.9 shows the characteristic Au and Fe XRD peaks. When the two figures are compared, although the Au and Fe3O4 peaks are present, the information is not sufficient to differenciate between the coexistence of gold and magnetite and gold coating the magnetite nanoparticles.

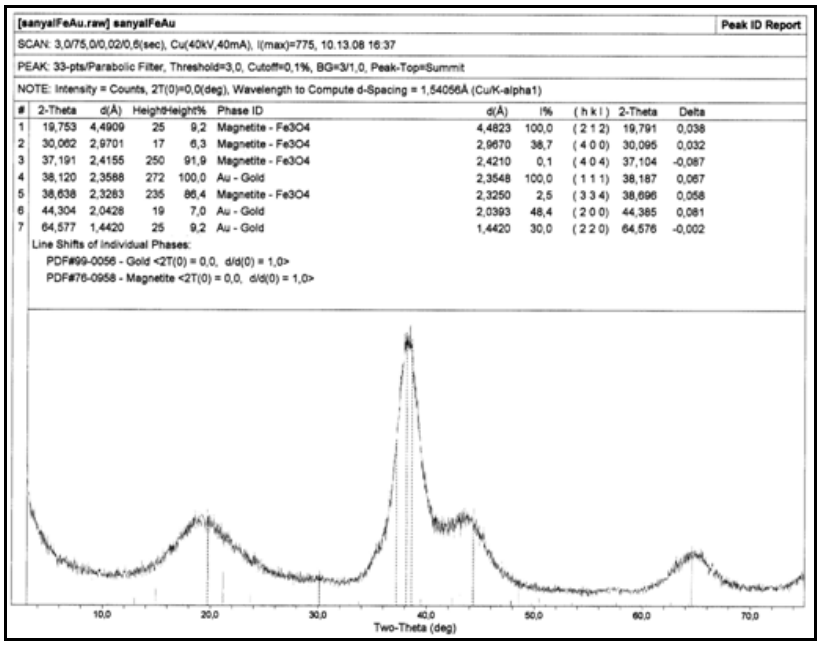

Figure 4.8. XRD graph of gold coated hydrophobic MNPs

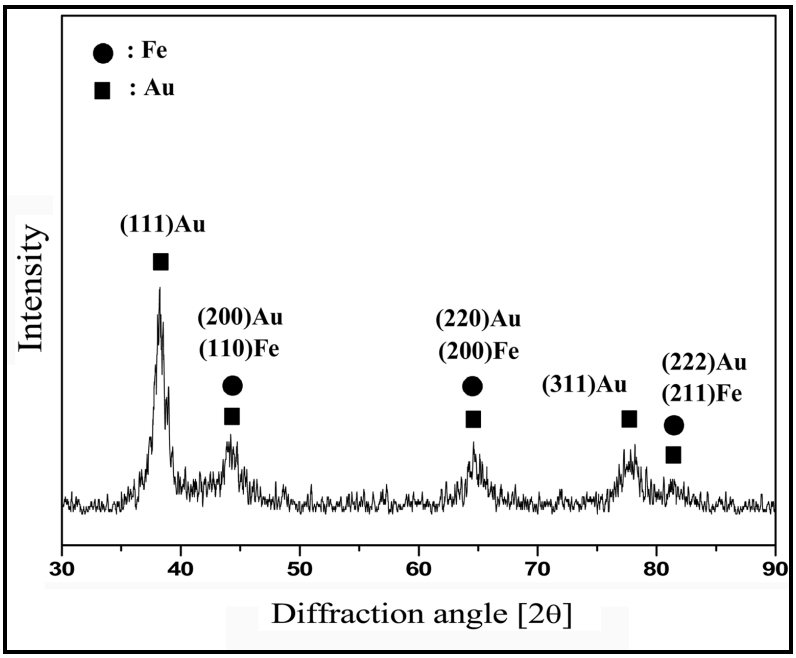

Figure 4.9. XRD peaks of Au-Fe

4.7. CONCLUSION

As described briefly in the Theoretical Background section there are several synthesis methods for preparing MNPs. However, a few of them were applied and given in this chapter. According to the characterization techniques MNPs are in size ranges of 5 nm to 9 nm and average hydro dynamic diameters for first and second step are nearly 11 nm and 16 nm respectively. Particles are also spherical in shape. The obtained particles are then used for the micropatterning experiments.

5. MICROPATTERNING OF SYNTHESIZED MNPs

In this chapter, the drying pattern of hydrophobic MNPs was investigated with different parameters such as solvent, magnetic field gradient applied, template, etc.

$$F_m - V_{particle} \times \chi \times \mu_0 \times H \times \nabla H \quad (5.1)$$

Equation 5.1 shows the Kelvin force in which $V_{particle}$, χ, μ_0, H, ∇H and F_m parameter are the volume of the MNP, susceptibility of MNP, vacuum permeability, magnitude of magnetic field and magnetic field gradient and the force exerted by a magnetic field to a MNP, respectively. This equation shows how these parameters are affecting the force acting on each particle [107, 108]. The susceptibility was related to the material of the particles which was Fe_3O_4. The diameters of the NPs had been characterized in TEM and observed that size distribution was narrow by DLS. Therefore, the volume of the MNPs was known and assumed to be constant. The remaining parameters affecting the force acting on a MNP were the magnitude of the applied magnetic field and the magnetic field gradient. By changing the values of the magnetic field and magnetic field gradient, force acting on a MNP could have been altered. In the experiments, magnetic field was created by the Neodymium handheld magnet, generating magnetic field of 0.1 T. Also there were two different types of MNPs were used. First one was the magnetite beads (MB) with –COOH group attached which was purchased from Ademtech. The other one was the synthesized hydrophobic MNPs. In order to increase the magnetic field gradient, MBs were used in the template preparation so that the effect of magnetic field gradient could be observed.

5.1. TEMPLATE PREPARATION

Compact Disc (CD) was used as the template because it has approximately 900 nm-channels. By using convective assembly set-up which can be seen in Figure 5.1, the channels of the CD were filled with MBs. CD was fixed on the moving stage. A clean glass slide was placed on top of the fixed CD with an angle approximately 30º. The glass slide was held by a clamp at this particular angle. The solution containing MNPs that was

to be assembled is spotted at the junction point of two slides. As the stage moves forward, the solution at the junction point was spreaded on the clean glass slide or CD surface. As the suspension of MNPs spread, the solvent starts to evaporate, leaving the MNPs to assemble on the CD.

The parameters affecting the convective-assembly method are the stage velocity, loaded suspension volume and concentration of the suspension and the angle of the two glass slides. Convective assembly set up is shown in the Figure 5.1. Optimal conditions were found by Deniz Sandal who was an MSc student in the Department of Genetics and Bioengineering.

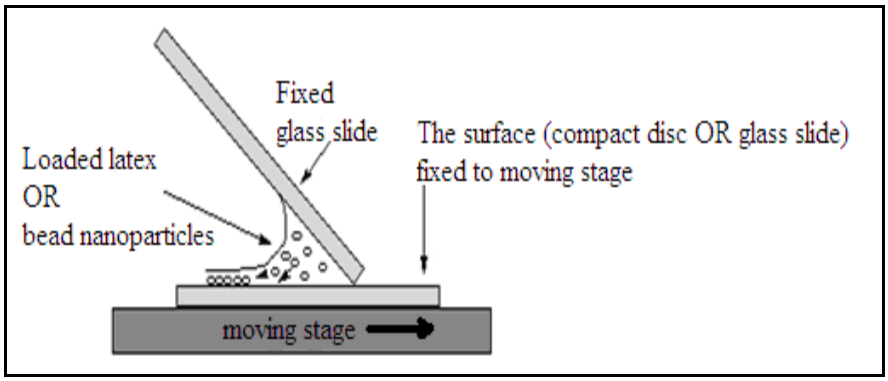

Figure 5.1. The convective-assembly set up [54]

5.2. TEMPLATING STUDIES

In this section, the presence of a patterned surface between a magnetic field and the substrate that the MNPs were assembled on was investigated. Figure 5.2 (A-D) demonstrates the experimental procedure up to the magnetic field studies. The prepared surface (A), with beads assembled into the microchannels (B), was coated with a thin film of PDMS (C). Then, the MNPs were dropped on the PDMS (D) in the absence and presence of magnetic field that was created by a hand held magnet approximately having magnetic field of 103.9 mT. The influence of solvent types on forming MNPs structures was also studied. Furthermore, not only the PDMS covered patterned CD surfaces but also

untreated CD surfaces and patterned but not PDMS covered surfaces were studied. The resulting surfaces were characterized by using SEM.

The hydrophobic MNPs were suspended in hexane, heptane and decane and the concentration was determined to be 0.008 g/mL by using Tiron test.

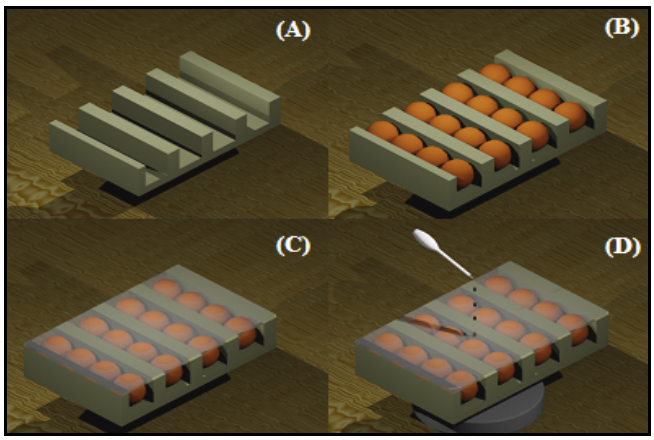

Figure 5.2. The schematic representation of the overall experiments: a. the CD template having microchannels, b. assembled beads into the microchannels, c. covered substrate with a thin film o f PDMS, d. dropping MNPs under the magnetic field [54]

5.3. CHARACTERIZATION OF MICROPATTERNED MNPS

5.3.1. MNP Solution on Untreated CD Surface

MNPs which were suspended in n-heptane and n-decane were dropped on original CD without aluminum foil on the surface of it. The dropping experiments were done both in the presence and absence of magnetic field.

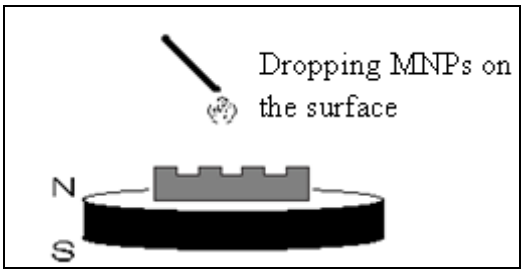

Figure 5.3. Side view of CD on top of a magnet

The SEM images of n-heptane suspension of MNPs in the presence of magnetic field can be seen from the Figure 5.4. It was observed that the MNPs were assembled in the sub-layers but at some places aggregation was recognized.

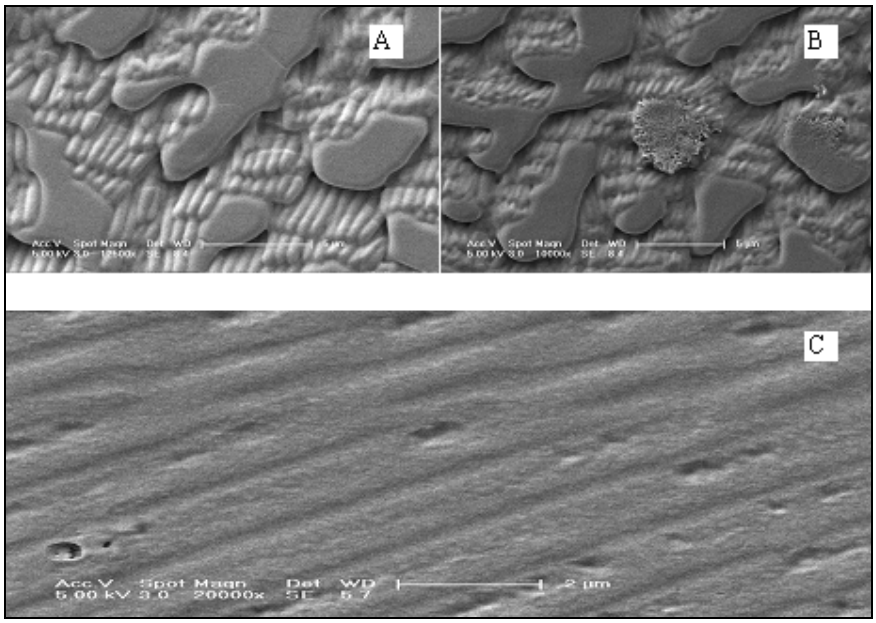

Figure 5.4. MNPs suspended in n-heptane on untreated CD (magnetic field on) a. and b. rod shape microstructures with agglomerations, c. assembled MNPs in the sublayers

In Figure 5.5, n-heptane suspension of MNPs on untreated CD in the absence of magnetic field can be seen. Contrary to Figure 5.4, no significant structure formation from MNPs was observed. As a result, only in the presence of external magnetic field, MNPs self assemble to form larger structures.

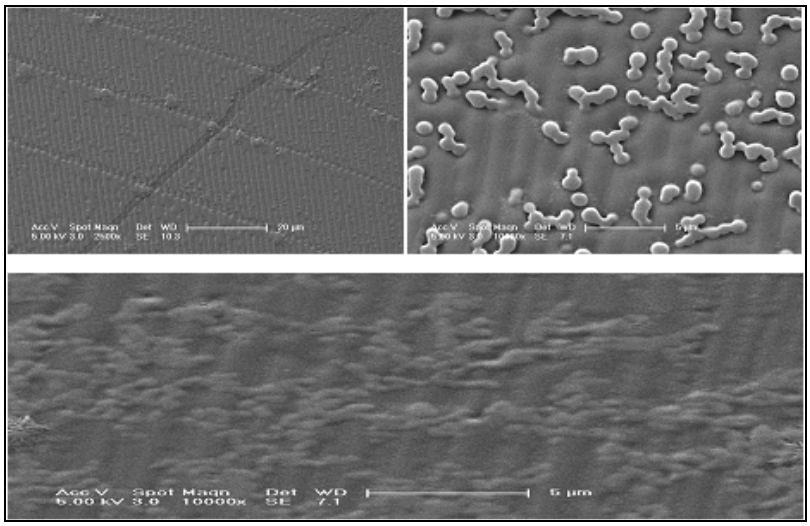

Figure 5.5. MNPs suspended in n-heptane on untreated CD (magnetic field off)

The same procedure was repeated for the n-decane suspension of MNPs. SEM image of the dried pattern can be seen in Figure 5.6.

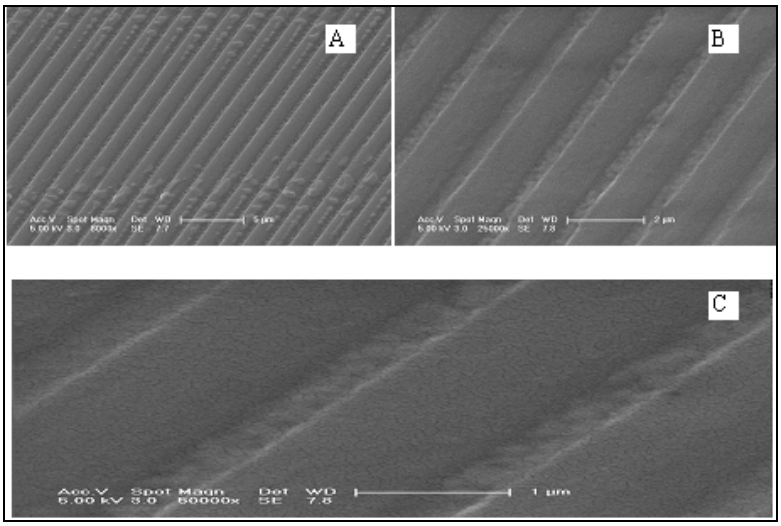

Figure 5.6. MNPs suspended in n-decane on untreated CD (magnetic field on)

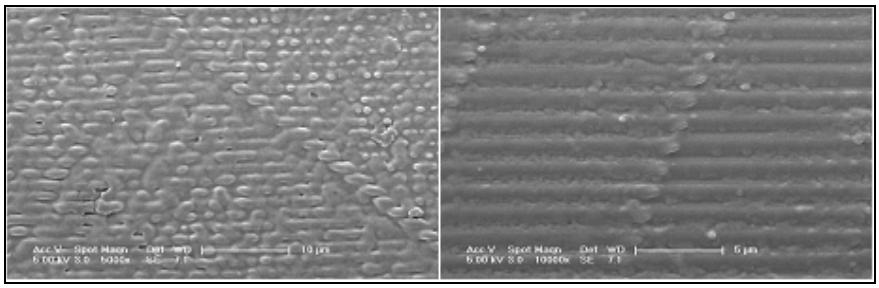

Figure 5.7. MNPs suspended in n-decane on untreated CD (magnetic field off)

In the Figures 5.6 and 5.7, the n-decane suspensions of MNPs in the presence and absence of magnetic field can be seen. Opposite to n-heptane suspension no significant structure formation was observed in the presence of magnetic field. However, some MNP agglomeration in the absence of magnetic field was observed while the microchannels of the CD were filled with MNPs in the presence of an external magnetic field.

5.3.2. MNP Drop Casting on Patterned CD

The microchannels of CD were filled with MBs by using convective assembly set-up and used as the template. Schematical representation of the experimental set up is shown in the Figure 5.8. Figure 5.9 shows the SEM image of the MBs in the microchannels of CD. They were used as the template as prepared. The n-heptane suspension of MNPs was dropped on this template in the absence and presence of magnetic field.

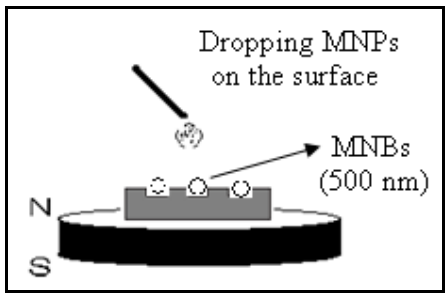

Figure 5.8. Side view of CD with MBs on top of a magnet

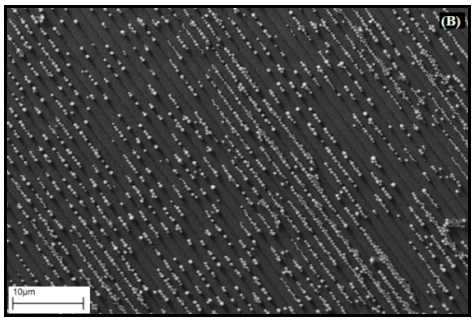

Figure 5.9. MBs in the microchannels

In the Figure 5.10, MBs and the microchannels of CD can be seen. Since MBs were not fixed in the channels after patterning with convective assembly, when the magnetic field was applied MBs moved out of the channels and formed clusters.

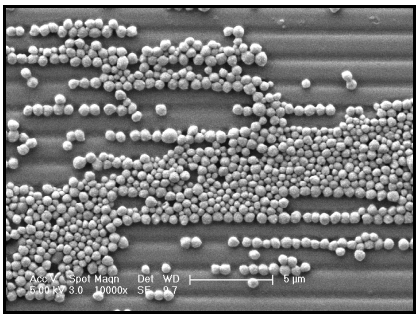

Figure 5.10. MBs on CD (magnetic field on)

Addition of MNPs onto the MBs results in MNPs preferential aggregation on MBs as seen in Figure 5.11.

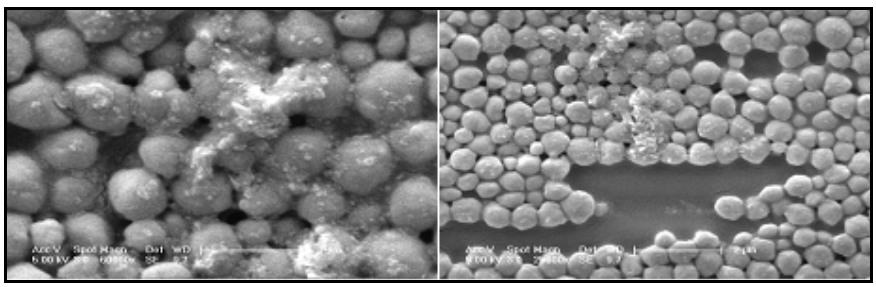

Figure 5.11. MNPs suspended in n-heptane on MBs (magnetic field on)

When the magnetic field was not applied, the images of MNPs in the presence of MBs on CD are given in the Figure 5.12. As it can be seen from the figure most of the MBs stay in the microchannels which can be due to the absence of magnetic field. Furthermore MNPs were dried randomly without a particular preference for MBs.

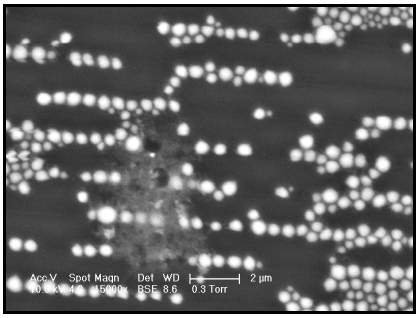

Figure 5.12. MNPs suspended in n-heptane on MBs (magnetic field off)

5.3.3. MNP Drop Casting on Patterned CD with PDMS

Although the channels were successfully filled with MBs, it was shown that they move upon application of an external field. In order to fix the MBs inside the channels, a top layer of PDMS was used. MBs were filled into the microchannels of CD using convective assembly set-up and a thin layer of PDMS was then used to cover this surface. Experimental set up for the drop casting study is shown in the Figure 5.13.

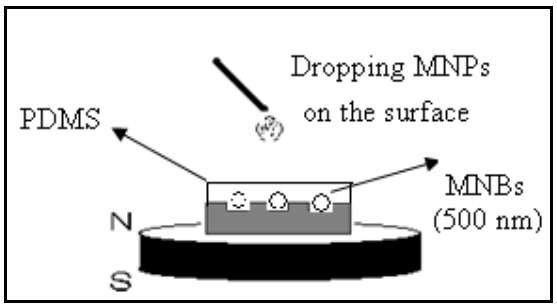

Figure 5.13. Side view of CD with MBs fixed with PDMS on top of a magnet

Figure 5.14 shows the MBs in the microchannels of CD and the PDMS covered MBs. As it can be seen from the Figure 5.14 B, when CD covered with PDMS, MBs can

not be seen. This result provides that when the MNPs suspension is dropped on this template, the observable microstructures solely consist of MNPs.

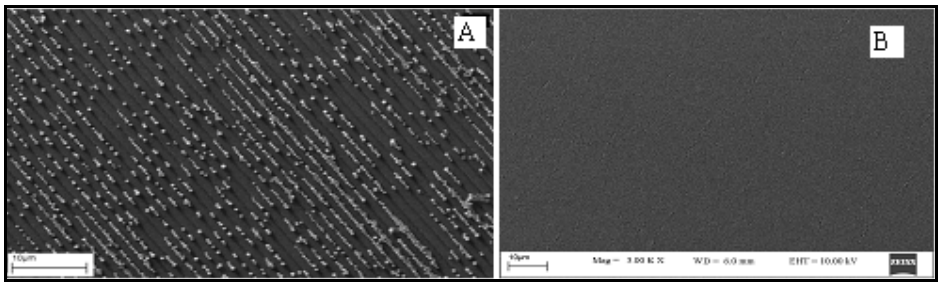

Figure 5.14. a. MBs in the microchannels, b. MBs covered with PDMS

To this template n-heptane suspension of MNPs was dropped when magnetic field was on and the SEM image after drying is given in the Figure 5.15. It can be seen that the MNPs do not form the channel shape structures as it was expected but instead, rod shape microstructures mostly with spherical cross sections were observed pointing the same direction. In section 2.2.1 the behavior of MNPs during the presence of magnetic field was mentioned, according to that the vertical direction of rod shape structures were observed as expected since the direction of magnetic field is perpendicular to the template.

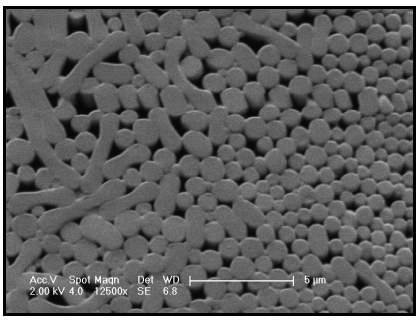

Figure 5.15. MNPs suspended in n-heptane on CD (patterned MBs covered with PDMS) (magnetic field on)

Figure 5.16 shows also SEM image of n-heptane suspension of MNPs dropped on the same template. The occurred structures were observed as rod shape structures and their

diameter and height were measured as 330 nm and 1.25 µm, respectively. According to the elemental analysis, those structures were confirmed to be only Fe_3O_4.

Figure 5.16 shows also SEM image of n-heptane suspension of MNPs dropped on the same template. The occurred structures were observed as rod shape structures and their diameter and height were measured as 330 nm and 1.25 µm, respectively. According to the elemental analysis, those structures were confirmed to be only Fe_3O_4.

Based on the observed structures in the Figures 5.15 and 5.16, it can be seen that the MBs underneath the PDMS increases the magnetic field gradient as expected. According to the equation 5.1, it was known that as the magnetic field gradient increases the force acting on each particle increases.

In the Figure 5.16 there are horizontal structures at the edges, the reason for that may be, these structures can be outside the magnetic field or the MB pattern.

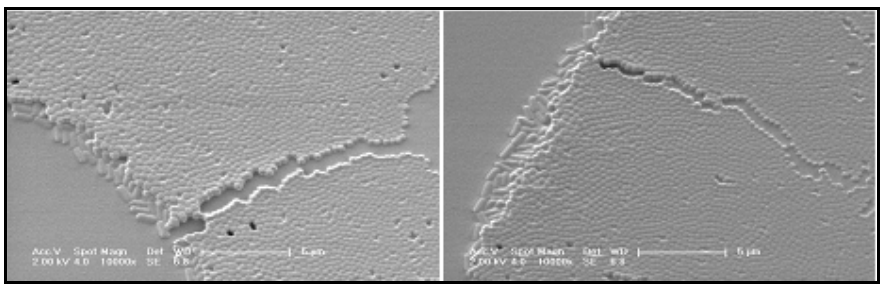

Figure 5.16. MNPs suspended in n-heptane on CD (patterned MBs covered with PDMS) (magnetic field on)

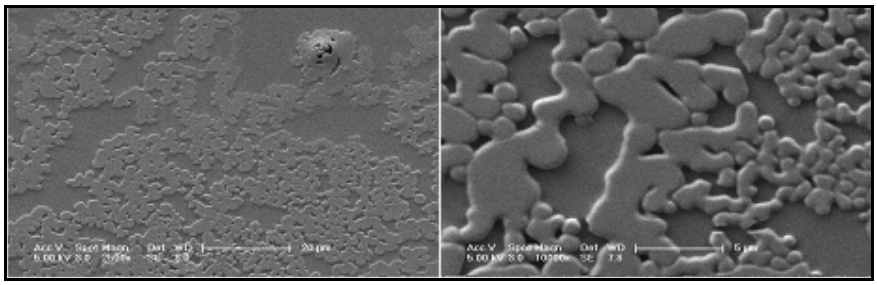

Figure 5.17. MNPs suspended in n-heptane on CD (patterned MBs covered with PDMS) (magnetic field off)

The image in the Figure 5.17 was obtained when the suspension of MNPs in n-heptane was dropped on the same template and dried without a magnetic field. Unlike Figure 5.16, it was observed that in the systems without magnetic field, MNPs drying in a random fashion without forming higher structures.

The same procedure was repeated for the n-decane suspension of MNPs to see effect of drying rate on the forming structures. SEM images of the occurred structures can be seen from the Figure 5.18.

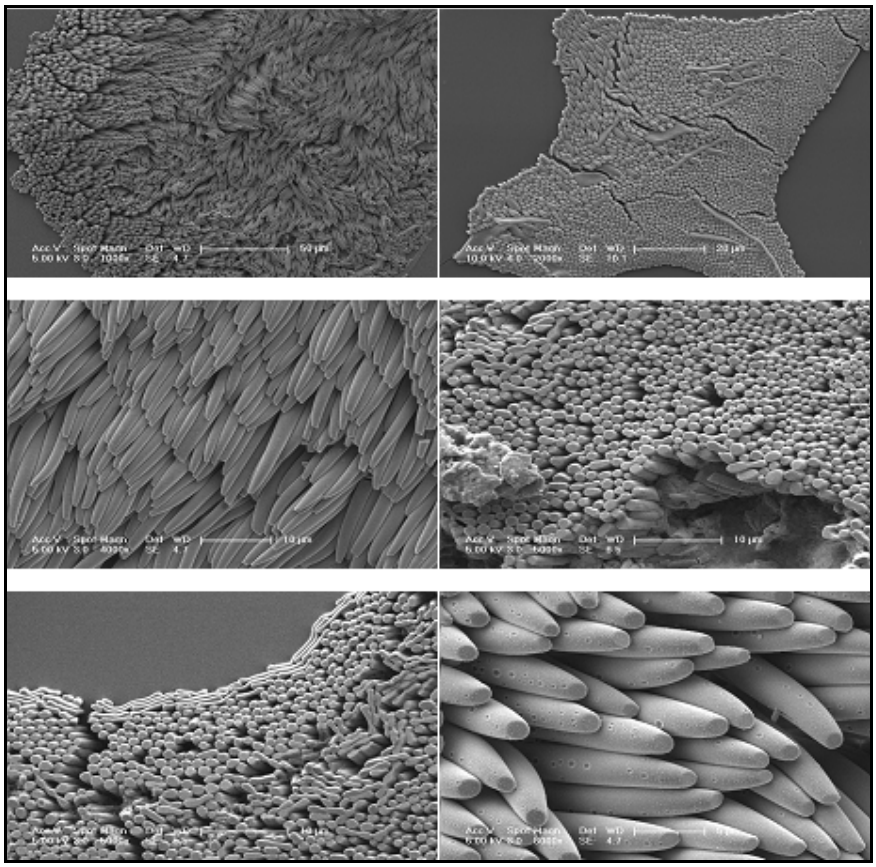

Figure 5.18. MNPs suspended in n-decane on CD (patterned MBs covered with PDMS) (magnetic field on)

Also, from Figure 5.19 it can be seen that the cross-section of the structures are not hollow.

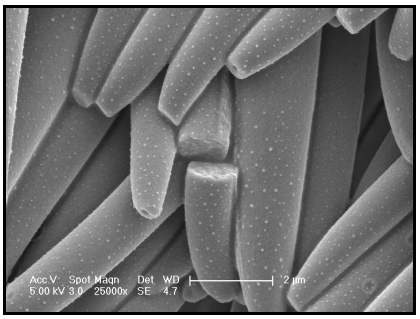

Figure 5.19. MNPs suspended in n-decane on CD (patterned MBs covered with PDMS) (magnetic field on)

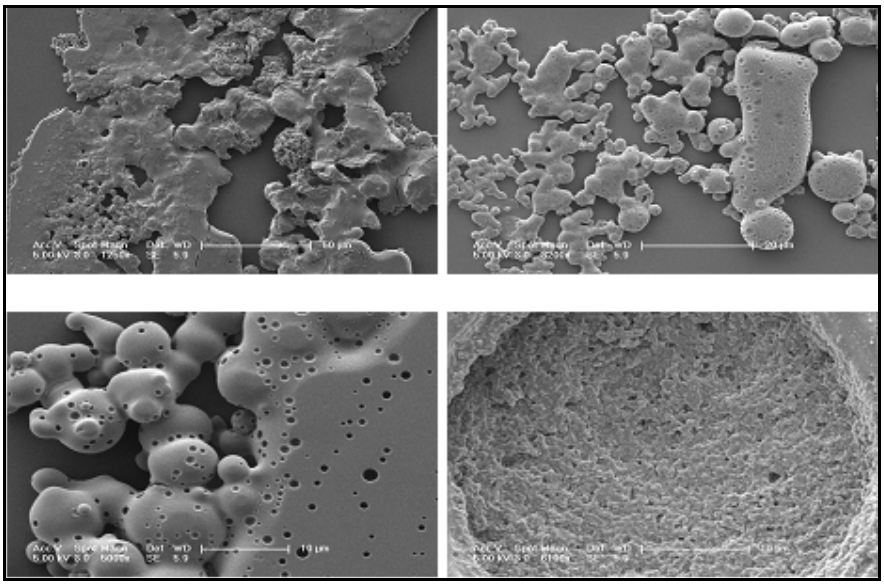

Figure 5.20. MNPs suspended in n-decane on CD (patterned MBs covered with PDMS) (magnetic field off)

When the same procedure was repeated for the MNPs suspended in n-decane when magnetic field off, no regular structure occurs as it can be seen from the Figure 5.20.

Furthermore, the same procedure was applied to the hexane suspension of MNPs both in the presence and absence of magnetic field. However, no regular structures were observed as it can be seen from the Figures 5.21 and 5.22. This can be due to the fast evaporation rate of hexane when compared with n-heptane and n-decane. Since the evaporation rate is higher, there is not sufficient time for the NPs to organize themselves into such high structures.

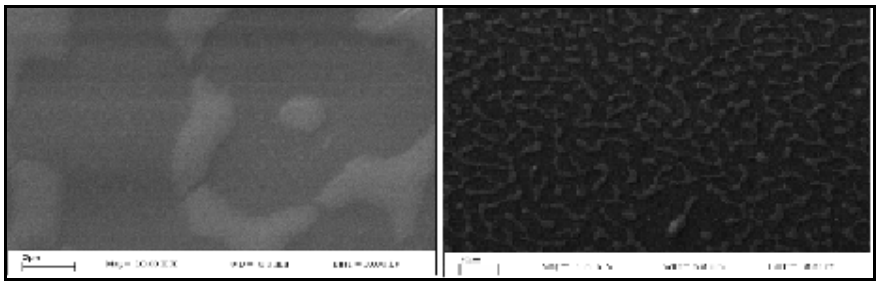

Figure 5.21. MNPs suspended in n-hexane on CD (patterned MBs covered with PDMS) (magnetic field on)

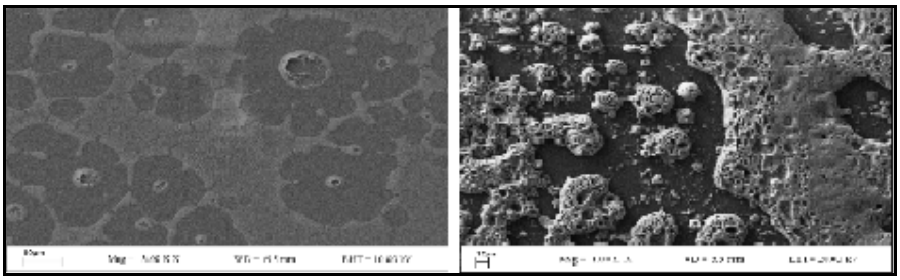

Figure 5.22. MNPs suspended in n-hexane on CD (patterned MBs covered with PDMS) (magnetic field off)

Also, hydrophilic MNPs were dropped on the same template with MBs covered with PDMS and left to dry. However, as it can be seen from the Figure 5.23, pattern can not be formed. Since, the PDMS surface is hydrophobic; the wettability of the surface is rather poor for the MNPs suspended in water. Therefore, the MNPs suspended in water caused the uncontrolled aggregation of MNPs on PDMS surfaces. This system was not further investigated.

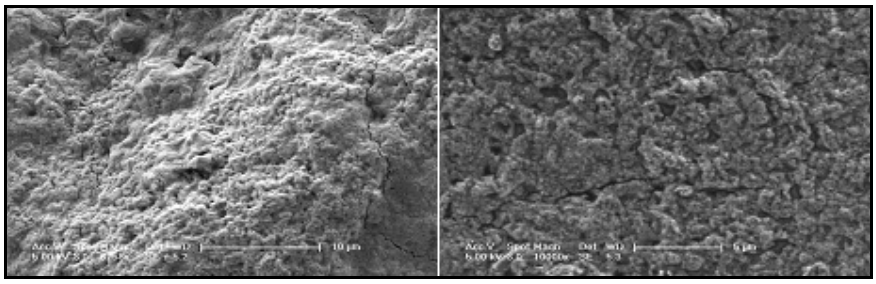

Figure 5.23. MNPs in water on CD (patterned MBs covered with PDMS) (magnetic field on)

5.3.4. Gold Coated MNP Drop Casting on Patterned CD with PDMS

Gold coated MNPs were also dropped on the patterned CD which was covered with PDMS in order to see both the similarities and the differences between the formed structures of gold coated MNPs and MNPs. Figure 5.24 shows the SEM images gold coated MNPs suspended in n-decane on patterned CD with PDMS. It was observed that the formed structures were different than the MNPs because the surfaces of the formed structures with the gold coated MNPs were not smooth while they were smooth with MNPs. With the help of these images it was thought that instead of gold coating of MNPs, maybe both MNPs and gold NPs were formed during the synthesis.

Also the horizontal structures were observed with the drop casting study of n-decane suspension of gold coated MNPs, while the n-decane suspension of MNPs leads to perpendicular structures. The effect of magnetic field on the MNPs may be decreased when they were covered with gold or when there are gold NPs present in the medium. Another important observation is that the surfaces of these larger structures are not as smooth as those obtained by magnetite. If the gold was co-suspended along with magnetite in solution, what is observed as roughness may simply be gold nanoparticles precipitating on magnetite during solvent evaporation. At this point, it not possible to suggest a definitive explanation on the surface roughness.

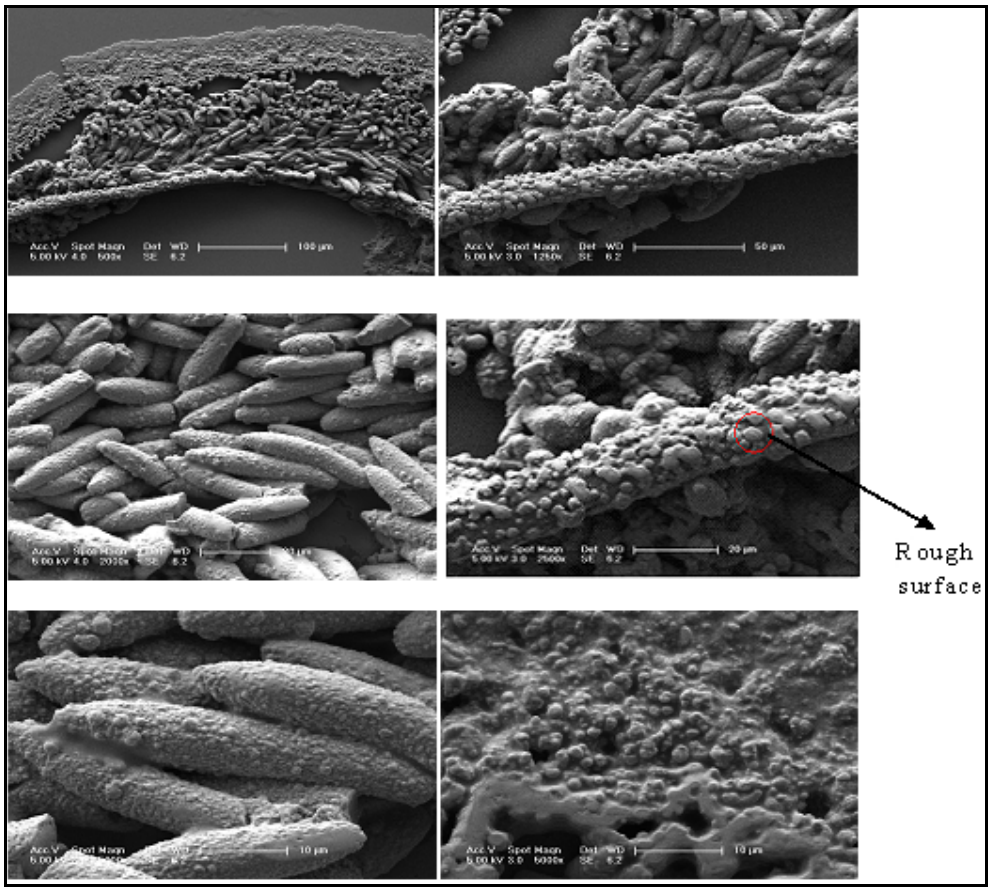

Figure 5.24. Gold coated MNPs in n-decane on CD (patterned MBs covered with PDMS) (magnetic field on)

When the magnetic field is off, arranged structure can not be observed as it can be seen from the Figure 5.25.

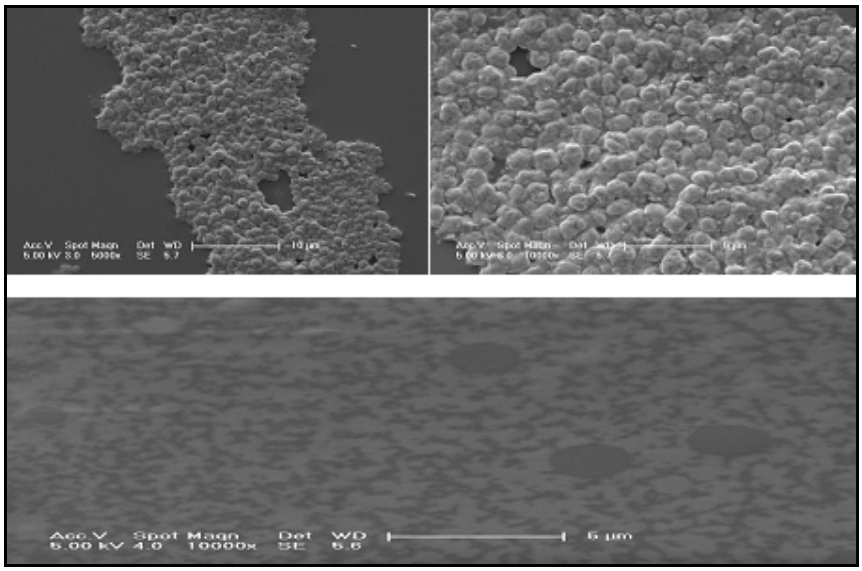

Figure 5.25. Gold coated MNPs suspended in n-decane on CD (patterned MBs covered with PDMS) (magnetic field off)

5.4. CONCLUSION

Synthesized hydrophobic MNPs and gold coated MNPs which were given in Chapter 4 were used for the patterning experiments. The aim of this study was to obtain well defined higher structures. This was done by comparing different templates with different solvents both in presence and absence of magnetic field. It was observed that higher structures can be obtained by using non-polar solvents. Hexane, heptane and decane were investigated as solvents. However, when an external magnetic field was applied, microstructures from only heptane and decane (not from hexane) suspensions in the presence of MBs were observed. This is possibly due to the fast evaporation rate of hexane because the evaporation rate of hexane is approximately 9 times faster compared to normal Butyl Acetate standard and due to this fast evaporation rate, there is not sufficient time for the NPs to organize themselves into such high structures. Also, heptane evaporation rate is 5 times faster than normal Butyl Acetate standard and decane evaporation rate is even slower than (0.07) normal Butyl Acetate standard.

Also when the templates with and without MBs were compared, it was observed that MBs underneath the PDMS increases the magnetic field gradient resulting in a higher force acting on magnetic particles leading to more organization of particles.

Furthermore, when gold coated magnetic nanoparticle suspension was used, also formed structures were also observed but surface roughness was different when compared with MNP suspension. With the help of this observation it was thought that instead of gold coating of MNPs, may be both MNPs and gold NPs were formed during the synthesis. These particles should be characterized better and this part of the work requires further investigation.

6. CONCLUSION and RECOMMENDATIONS

6.1. CONCLUSION

The aim of this study was to prepare well-defined magnetic surfaces and to investigate their use as chemical and biological sensors.

In order to fulfill the aim, first of all MNPs were synthesized in both water and oil phases. They were characterized by using DLS, TEM and XRD. For the hydrophobic MNPs, it was found that they are in spherical shapes with a hydrodynamic diameter approximately 6 nm.

Hydrophobic MNPs were then coated with gold because gold improves the effect of magnetite especially for the biomedical applications. Gold coated MNPs were then characterized by XRD and although XRD pattern of gold was observed along with Fe_3O_4 pattern, it is not possible to distinguish from XRD data whether gold is in coexistence with Fe_3O_4 or it actually coats the MNP surface.

For the patterning experiments, compact disc was used because it has microchannels on the surface. Two types of magnetic particles were used during the investigation; first one was the MBs (500 nm) and the second one was the synthesized MNPs (~6 nm). After removing the aluminum foil from the surface of the CD, microchannels of CD were filled with MBs by using convective assembly set-up. Then in order to fix the positions of MBs, the surface was covered with PDMS. As described in the chapter 5, the MNPs with various organic solvents were dropped on top of the template by either using magnetic field or not and they were left to dry. The obtained surfaces were then characterized by SEM. When an external magnetic field was applied, microstructures from the heptane and decane suspensions but not from hexane suspension in the presence of MBs were observed. It was thought that this is due to the fast evaporation rate of hexane (i.e. 9 times faster compared to normal Butyl Acetate standard). Due to this fast evaporation rate, there is not sufficient time for the NPs to organize themselves into such high structures. Also, it was observed that when decane and heptane were used different types of structures formed as expected.

Again this may be because of the different evaporating rates of these organic solvents. In all cases, no particular structure was observed in the absence of the applied magnetic field.

The same procedure was repeated for the gold coated MNPs. It was expected that the structures that formed with gold coated MNPs would be similar to those with MNPs. However, the observed structures were different. Also, with the help of the SEM images it was thought that instead of gold coating of MNPs, may be both MNPs and gold NPs were formed during the synthesis.

As a conclusion, well defined magnetic structures of micron sizes were formed through self assembly of synthesized MNPs.

6.2. RECOMMENDATIONS

In this work, CD was used as a template for MBs assembly. Instead of using CD, a different template may be used which have a different pattern on its surface. For example monolayer may be formed with MBs so that the enhancement of magnetic field gradient with MBs can be further proved and there would be a chance to see the difference.

Furthermore, since the MNPs arrange themselves in the magnetic field lines to form structures, may be different position of magnetic field could be applied.

Since during the experiments magnetic field was kept constant, the effect of magnetic field could not been observed. The work could be done by varying the magnetic field strength.

Moreover instead of using only PDMS different material could also be tried to see the change in the magnetic field gradient which is directly proportional with the magnetic force acting on individual particles.

Also, may be different magnetic material could be used to see the effect of magnetic susceptibility of the particles.

This work has great potential in creating micron sized magnetic materials composed of superparamagnetic NPs. Therefore, further studies should be carried out to obtain structures of desired shape and size as well as properties.

REFERENCES

1. Madou, M.J., *Fundamentals of Microfabrication: The Science of Miniaturization*, 2001.

2. Cavallini, M., P. Stoliar, J. F. Moulin, M. Surin, P. Leclere, R. Lazzaroni, D. W. Breiby, J. W. Andreasen, M. M. Nielsen, P. Sonar, A. C. Grimsdale, K. Mullen and F. Biscarini, "Field-Effect Transistors Based on Self-Organized Molecular Nanostripes", *Nano Lett.***,** Vol. 5, pp. 2422–2425, 2005.

3. Cavallini, M., J. Gomez-Segura, D. Ruiz-Molina, M. Massi, C. Albonetti, C. Rovira, J. Veciana and F. Biscarini, "Magnetic Information Storage on Polymers Using Patterned Single-Molecule Magnets", *Angew. Chem. Int*, Vol. *44*, pp. 888-892, 2005.

4. Hafeli, U.O. and G.J. Pauer, "In Vitro and in Vivo Toxicity of Magnetic Microspheres", *Magn. Magn. Mater.*, Vol. 194, pp. 76-82, 1999.

5. Shinkai, M., "Functional Magnetic Particles for Medical Applications", *Biosci. Bioeng.*, Vol. 94, pp. 606-613, 2002.

6. Mornet, S., Vekris, A., Bonnet, Duguet, J. E., Grasset, F., Choy, J. H., Portier, J. DNA–Magnetite Nanocomposite Materials, *Mater. Lett.* **2000,** *42*, 183–188.

7. Gupta, A. K. and M. Gupta, "Cytotoxicity Supression and Cellular Uptake Enhancement of Surface Modified Magnetic Nanoparticles", *Biomaterials,* Vol. 26, pp. 1565-1573, 2005.

8. Palacin, S., P. C. Hidber, J-P. Bourgoin, C. Miramond, C. Fermon, and G. M. Whitesides, “Patterning with Magnetic Materials at the Micron Scale”, *Chem. Mater.*, Vol. 8, pp. 1316-1325, 1996.

9. Xue, W., T. H. Cui, X. J. Lei, D. B. Li, R. Shao, and D. A. Bonnell, “In situ Deposition/Positioning of Magnetic Nanoparticles with Ferroelectric Nanolithography”, *J. Mater. Res.*, Vol. 20, pp. 712-718, 2005.

10. Erokhina, S., T. Berzina, L. Cristofolini, D. Shchukin, G. Sukhorukov, G. L. Musa, V. Erokhin, and M.P. Fontana, “Patterned Arrays of Magnetic Nano-Engineered Capsules on Solid Supports”, *J. Magn. Magn.Mater.*, Vol. 272, pp. 1353-1354, 2004.

11. Anders, S., S. Sun, C. B. Murray, C. T. Rettner, M. E. Best, T. Thomson, M. Albrecht, J. U. Thiele, E. E. Fullerton, and B. D. Terris, “Lithography and Self-Assembly for Nanometer Scale Magnetism”, *Microelectron. Eng.*, Vol. 61, pp. 569-575, 2002.

12. Furst, E.M., C. Suzuki, M. Fermigier, and A. P. Gast, “Permanently-linked Monodisperse Paramagnetic Chains”, *Langmuir*, Vol. 14, pp. 7334-7336, 1998.

13. Niu, H., Q. Chen, M. Ning, Y. Jia, and X. Wang, “Synthesis and One-Dimensional Self-Assembly of Acicular Nickel Nanocrystallites under Magnetic Fields”, *J. Phys. Chem. B,* Vol. 108, pp. 3996-3999, 2004.

14. Sheparovych, R., Y. Sahoo, M. Motornov, S. Wang, H. Luo, P. N. Prasad, I. Sokolov, and S. Minko, “Polyelectrolyte Stabilized Nanowires from Fe_3O_4 Nanoparticles via Magnetic Field Induced Self-Assembly”, *Chem. Mater.*, Vol. 18, pp. 591-593, 2006.

15. Vuppu, A. K., A. A. Garcia, and M. A. Hayes, "Video Microscopy of Dynamically Aggregated Paramagnetic Particle Chains in an Applied Rotating Magnetic Field", *Langmuir*, Vol. 19, pp. 8646-8653, 2003.

16. Caruntu, D., G. Caruntu, and C. J. O'Connor, "Magnetic Properties of Variable-Sized Fe_3O_4 Nanoparticles Synthesized from Non-Aqueous Homogeneous Solutions of Polyols" *J. Phys. D: Appl. Phys.* Vol. 40, pp. 5801-5809, 2007.

17. Awschalom, D. D. and D. P. Divencenzo, "Complex Dynamics of Mesoscopic Magnets", *Physics Today*, Vol. 48, pp. 43-48, 1995.

18. Suneel, S. D., *Synthesis And Processing Of Nano Powders*, 2009.

19. Woodrow Wilson International Center, *Managing The Effects of Nanotechnology – Characteristics, Definition and the Lack of Data About The Effects of Nanotechnology*, 2006.

20. Sugunan, A. and J. Dutto, *Nanoparticles for Nanotechnology,* 2004.

21. Kazuya N., Y. Hu, O. Uzun, O. Bakr, and F. Stellacci, *Chains of Superparamagnetic Nanoparticles*, 2008.

22. Shubayev, V. I., Pisanic, T. R. and J. Sunghoi, "Magnetic Nanoparticles for Theragnostics", *Advanced Drug Delivery Reviews,* Vol. 61, No. 6, pp. 467-477, 2009.

23. Teja, A. S. and P.Y. Koh, “Synthesis, properties, and applications of magnetic iron oxide nanoparticles”, *Elsevier*, Vol. 55, pp. 22-45, 2009.

24. Gupta, A. K. and Gupta, M. “Synthesis and surface engineering of iron oxide nanoparticles for biomedical applications”, Science Direct, Vol., *26*, 3995-4021, 2005.

25. Wilson, T. V., *Magnetorheological Fluids*, http://science.howstuffworks.com/liquid-body-armor2.htm, 2007.

26. Wilkerson, J., *Superparamagnetism*, http://isites.harvard.edu/fs/docs/icb.topic86897. Files/October_13_Temperature/Superparamagnetism_Wiki.pdf, 2006.

27. Pickler, C. and N. Edelman, *Determining the Curie and Neel Temperature of Minerals*, 2009.

28. Tartaj, P., M. P. Morales, S. V.-Verdaguer, T. Carreno and C. Serna, *The preparation of magnetic nanoparticles for applicatios in biomedicine*, 2003.

29. Giersig, M. and M. Hilgendorff, *Magnetic Nanoparticle Superstructures*, 2005.

30. Malvern Instruments Ltd., *Surfactant micelle characterization using dynamic light scattering*, 2006.

31. Sun, S., Zeng, H., Robinson, D. B., Raoux, S., Rice, P.M., Wang, S. X., Li, G. Monodisperse MFe2O4 (M = Fe, Co, Mn) Nanoparticles, *JACS*, **2004**, *126*, 273-279.

32. Lee, J. Y., *Colloidal Solutions,* http://cheed.nus.edu.sg/~cheleejy/index.html, 2010.

33. Mayes Research Group, *Molecularly Imprinted Core-Shell Nanoparticles,* http://www.uea.ac.uk/~c016/coreshell.htm, 2008.

34. Sounderya, N. and Y. Zhang, *Use of Core/Shell Structured Nanoparticles for Biomedical Applications,* 2008.

35. Pham, T. T. H., C. Cao and S. J. Sim, "Application of citrate-stabilized gold-coated ferric oxide composite", *Elsevier,* Vol. 320, pp. 2049–2055, 2008.

36. Xia, D., Li, D., Luo, Y. and S. R. Brueck, "An Approach to Lithographically Defined Self-Assembled Nanoparticle Films", *Advanced Materials,* Vol. 18, No. 7, pp. 930-933, 2006.

37. Wu, X. C., Chi, L. F. and H. Fuchs, "Patterning of Semiconductor Nanoparticles via Microcontact Printing", *European Journal of Inorganic Chemistry*, Vol. 2005, No. 18, pp. 3729-3733, 2005.

38. Kumar, S. and T. Nann, "Shape Control of II-VI Semiconductor Nanomaterials", *Small*, Vol. 2, No. 3, pp. 316-329, 2006.

39. Wang, X., Zhuang, J., Peng, Q. and Y. Li, "A General Strategy for Nanocrystal Synthesis", *Nature*, Vol. 437, No. 7055, pp. 121-124, 2005.

40. Murray, C. B., Norris, D. J. and M. G. Bawendi, "Synthesis and Characterization of Nearly Monodisperse CdE (E = sulfur, selenium, tellurium) Semiconductor Nanocrystallites", *Journal of American Chemical Society*, Vol. 115, No. 19, pp. 8706-8715, 1993.

41. Bönnemann, H. and R. Richards, "Nanoscopic Metal Particles - Synthetic Methods and Potential Applications", *European Journal of Inorganic Chemistry*, Vol. 201, No. 10, pp. 2455-2480, 2001.

42. Cai, Y. and B. Z. Newby, "Marangoni Flow-Induced Self-Assembly of Hexagonal and Stripelike Nanoparticle Patterns", *Journal of American Chemical Society*, Vol. 130, No. 19, pp. 6076-6077, 2008

43. Mulder, W. J. M., Koole, R., Brandwijk, R. J., Storm, G., Chin, P. T. K., Strijkers, G. J., Donega, C. M., Nicolay, K. and A. W. Griffioen, "Quantum Dots with a Paramagnetic Coating as a Bimodal Molecular Imaging Probe", *Nano Letters*, Vol. 6, No. 1, pp. 1-6, 2006.

44. Malvern Instruments Ltd, *Dynamic Light Scattering (DLS)*

http://www.malverninstruments.fr/LabFre/technology/dynamic_light_scattering/dynamic_light_scattering.htm, 2009.

45. Powder Technology Laboratory, *Mean Crystallite Size by X-Ray Diffraction (XRD)*, http://ltp.epfl.ch/webdav/site/ltp/shared/protocols/XRD_E.pdf, 2007.

46. Carter, C. W., *X-Ray Diffraction*, 2009.

47. FEI Company,

http://www.fei.com/uploadedFiles/Documents/Content/2006_06_AllYouWanted_pb.pdf, 2009.

48. Nobel WEB AB 2009,

http://nobelprize.org/educational_games/physics/microscopes/tem/index.html, 2009.

49. Buschow, K. H. J., *Handbook of Magnetic Materials*, Elsevier, Amsterdam, 2006.

50. Cruz, W. S., *Microscopy*,

http://www.nslc.wustl.edu/courses/Bio2960/labs/04Microscopy/microscopy.html, 2007.

51. Stenkamp, D. and P. Fruhstorfer, *EVO Series SEM Operator User Guide*, Carl Zeiss SMT Ltd, Cambridge, 2000.

52. Chunk, B. H., "Gold Nanocages Containing Magnetic Nanoparticles"

53. Cuyper, M. and S. J. H. Soenen, "Cationic Magnetoliposomes", Methods in Molecular Biology, Vol. 605, Chapter 6,

http://www.springerlink.com/content/u87mt87829r46306/fulltext.pdf, 2010.

54. Sandal, D. Ç., The Influence of Patterned Magnetic Beads on the Self-Assembly of Magnetic Nanoparticles , M.S. Report, Yeditepe University, 2009.